J. Fluid Mech. (1995), *vol.* 303, *pp.* 327–366

Instabilities and the formation of bubbles in fluidized beds

By K. ANDERSON, S. SUNDARESAN AND R. JACKSON
Department of Chemical Engineering, Princeton University, Princeton, NJ 08544, USA

(Received 3 November 1994 and in revised form 25 April 1995)

As is well known, most gas-fluidized beds of solid particles bubble; that is, they are traversed by rising regions containing few particles. Most liquid-fluidized beds, on the other hand, do not. The aim of the present paper is to investigate whether this distinction can be accounted for by certain equations of motion which have commonly been used to describe both types of bed. For the particular case of a bed of 200 μm diameter glass beads fluidized by air at ambient conditions it is demonstrated, by direct numerical integration, that small perturbations of the uniform bed grow into structures resembling the bubbles observed in practice. When analogous computations are performed for a water-fluidized bed of 1 mm diameter glass beads, using the same equations, with parameters modified only to account for the greater density and viscosity of water and to secure the same bed expansion at minimum fluidization, it is found that bubble-like structures cannot be grown. The reasons for this difference in behaviour are discussed.

1. Introduction

As soon as fluidized beds of solid particles began to be used technically it was observed that, on the whole, liquid-fluidized beds present a smooth appearance and expand progressively as the flow rate of fluid is increased, while gas-fluidized beds are traversed by rising pockets of gas which can be seen to burst through the surface, giving the bed the appearance of a boiling liquid. The terms 'particulate' and 'aggregative' were introduced to distinguish these types of behaviour, and a criterion to distinguish between them was proposed by Wilhelm & Kwauk (1948), who suggested that the bed behaves aggregatively if $Fr = u_m^2/gd_p > 1$, where u_m denotes the minimum fluidization velocity and d_p is the particle diameter. This criterion is purely empirical but some theoretical justification for its use was provided much later by a linear stability analysis of the ideal uniform fluidized state by one of the present writers (Jackson 1963*a*). This was based on continuity equations, and momentum equations of speculative form, and it predicted that all such beds should be unstable, with the dominant instability taking the form of plane waves with horizontal wavefronts rising through the bed. However, the rate of growth of these waves is found to be much larger in gas-fluidized beds than in beds of comparable particles fluidized by liquid so, in this sense, the former are much less stable than the latter. If one associates the instability with a tendency to form bubbles this suggests, though it certainly does not prove, that visible bubbles may be present in one case, but not the other.

This early analysis had the unsatisfactory feature of predicting that the rate of growth of the instabilities increases without bound as their wavelength tends to zero, which is clearly a consequence of omitting from the equations any terms representing

'viscous dissipation'. When such terms are introduced (Pigford & Baron 1965; Anderson & Jackson 1967, 1968) it is found that there is a dominant wavelength, for which the amplification rate is largest, but the bed always remains unstable unless an additional term, with the form of a pressure associated with the particle phase, is introduced. If this term increases sufficiently rapidly with increase in the concentration of particles, the bed may be stabilized (Garg & Pritchett 1975), so it seems possible that a stability criterion might serve to distinguish between aggregative and particulate behaviour. However, experiments (Anderson & Jackson 1969; El-Kaissy & Homsy 1976) show that liquid-fluidized beds of small glass beads, which are typically 'particulate' in behaviour, are not uniform and stable but are traversed by slowly developing rising waves closely resembling, in their initial stages of growth, the instability waves just described. A theoretical prediction of stability in these cases would, therefore, be unwelcome. Certain gas-fluidized beds of small particles, such as the fluid cracking catalyst used in oil refining (mean diameter approximately 60 μm), expand without bubbling or visible disturbance of any kind for some distance beyond the point of minimum fluidization, and there have been attempts to explain this in terms of the above stabilizing mechanism (Foscolo & Gibilaro 1984; Batchelor 1988). However, there is now compelling evidence that these expanded beds can bear limited stress without yielding (Mutsers & Rietema 1977; Tsinontides & Jackson 1993), and that it is the existence of this yield stress which is responsible for their stability.

The linear one-dimensional stability analyses just described serve to explain the existence of slowly growing waves in liquid-fluidized beds, and also why comparable waves in gas-fluidized beds grow much faster, but they have nothing to say about their ultimate fate and cannot explain why the waves in liquid-fluidized beds do not develop into bubbles, or whether the more unstable waves in gas-fluidized beds are, indeed, the precursors of bubbles. Over the intervening years there have been a number of attempts to extend the one-dimensional stability theory to take account of the nonlinearity of the equations of motion (Fanucci, Ness & Yen 1979; Liu 1982, 1983; Needham & Merkin 1983, 1986; Ganser & Drew 1990), but these have failed to show any qualitative distinction between the predicted behaviour of gas- and liquid-fluidized beds, and recent bifurcation analyses, again confined to one-dimensional motions (Dankworth & Sundaresan 1991; Göz 1992), also show no significant differences between the two cases. Secondary, two-dimensional instabilities of the one-dimensional wave pattern have been observed experimentally in water-fluidized beds (Didwania & Homsy 1981) and investigated theoretically by the same authors (Didwania & Homsy 1982) and by Needham & Merkin (1984), Batchelor & Nitsche (1991) and Batchelor (1993). These appear to play a role in a process that may lead to bubbles, but again the stability analyses are not able to predict the distinction in behaviour between gas- and liquid-fluidized beds. Thus, more than thirty years after linear stability analysis of proposed equations of motion revealed why ideal uniform fluidized beds are not generally observed, we still do not know whether these equations contain the physics needed to explain the spontaneous generation of bubbles, and to distinguish bubbling from non-bubbling systems.

By direct numerical integration of the equations of motion which had served as a basis for the stability analyses, propagating, bubble-like structures in fluidized beds were found as early as the 1970s (Pritchett, Blake & Garg 1978) and quite extensive comparisons of observed and computer-generated bubbles have been reported more recently (see, for example, Gidaspow, Syamlal & Seo 1986; Syamlal & O'Brien 1989; Kuipers 1990). However, of these only Syamlal & O'Brien reported any spontaneous bubble formation within a uniformly fluidized bed; otherwise the solutions represent

bubbles injected into the bed, or formed from a gas jet at the level of the distributor. We are not aware of any comparable computations for liquid-fluidized beds to resolve the observed differences between gas and liquid fluidization.

In this paper we will attack the problem of growing disturbances directly, by numerical integration of the equations of motion from given initial conditions. In principle, this would allow us to explore all aspects of the dynamical behaviour of fluidized beds, and how they depend on the form of the postulated equations of motion and the values of parameters in these equations. Howevever, our objective here is quite limited. We confine attention to just two unperturbed fluidized beds of hard monodisperse spherical particles: one bed typical of those gas-fluidized systems which are observed to bubble immediately the gas velocity exceeds that needed for minimum fluidization, and the other typical of liquid fluidized beds in which bubbles are not seen. A form of the equations of motion which has been used extensively in the literature referred to above (though never justified *a priori*) is adopted for both cases. The two beds are distinguished in the equations only by taking different values for obviously different physical properties, such as the particle diameter, the densities of the two materials and the viscosity of the fluid phase, and hence for quantities dependent on these, such as the terminal velocity of fall of an isolated particle. Since both gas- and liquid-fluidized beds of hard spheres have essentially the same volume fraction of solids at minimum fluidization, and minimum fluidization also marks the onset of instability, one other parameter in the equations is adjusted to make the volume fractions match for the two beds at their stability limits. It is then shown that small initial disturbances will grow into structures recognizably identifiable with bubbles when the gas-fluidized bed is expanded just beyond its stability limit, but this does not happen in the liquid-fluidized bed. On the basis of just two calculations it is not possible to draw conclusions of any generality about the factors which determine whether bubbles will form, but the solutions give some hint of the mechanical origin of the difference in behaviour.

2. Equations of motion

Equations of motion relate averaged velocities, concentrations, etc. of the two phases. Of course, in general there is no guarantee of the existence of closed relations between the averaged variables, but we assume that closure is possible for the problems of interest here. The variables in question may be defined as local time or spatial averages for the system of interest, or as averages over an ensemble of macroscopically equivalent systems. There is now an extensive and varied literature on the averaging process; see, for example, Anderson & Jackson (1967), Drew (1971), Drew & Segel (1971), Hinch (1977), Nigmatulin (1979), Joseph & Lundgren (1990), and Zhang & Prosperetti (1994).

The equations used here are those proposed by Anderson & Jackson (1967) and subsequently used in a number of the stability studies referred to above. They have the following form:

$$\frac{\partial \phi}{\partial t} + \nabla \cdot (\phi \boldsymbol{v}) = 0, \tag{1}$$

$$\frac{\partial (1-\phi)}{\partial t} + \nabla \cdot [(1-\phi)\boldsymbol{u}] = 0, \tag{2}$$

$$\rho_s \phi \frac{\mathrm{D}_s \boldsymbol{v}}{\mathrm{D}t} = -\nabla \cdot \boldsymbol{E}_s + \boldsymbol{F} + \phi(\rho_s - \rho_f)\boldsymbol{g} + \rho_f \phi \frac{\mathrm{D}_f \boldsymbol{u}}{\mathrm{D}t}, \tag{3}$$

and
$$\rho_f \frac{\mathrm{D}_f \boldsymbol{u}}{\mathrm{D}t} = -\nabla \cdot \boldsymbol{E}_f - F + \rho_f \boldsymbol{g}, \tag{4}$$

where (1) and (2) are continuity equations for the particles and the fluid, while (3) and (4) represent momentum balances for the two phases. ϕ is the volume fraction of solids, ρ_f and ρ_s are the densities of the fluid and solid materials, $\boldsymbol{u}$ and $\boldsymbol{v}$ are their local average velocities, $\boldsymbol{g}$ is the specific gravity force vector, $\boldsymbol{F}$ is the drag force, per unit bed volume, between the two phases, and $\boldsymbol{E}_f$ and $\boldsymbol{E}_s$ are stress tensors associated with the separate momentum balances The symbols $\mathrm{D}_f/\mathrm{D}t$ and $\mathrm{D}_s/\mathrm{D}t$ denote material time derivatives based on the velocities $\boldsymbol{u}$ and $\boldsymbol{v}$, respectively.

Empirical closure expressions for the drag force are available, but the two stress tensors are not known with any certainty. Here we adopt the simplest physically credible expression for each term, since part of our purpose is to see whether equations of motion of simple form can account for the distinction between bubbling and non-bubbling systems. Thus we take

$$\boldsymbol{F} = \beta(\boldsymbol{u} - \boldsymbol{v}), \tag{5}$$

$$\boldsymbol{E}_s = p_s \boldsymbol{I} - \mu_s [\nabla \boldsymbol{v} + \nabla \boldsymbol{v}^T - \tfrac{2}{3}(\nabla \cdot \boldsymbol{v}) \boldsymbol{I}], \tag{6}$$

$$\boldsymbol{E}_f = p_f \boldsymbol{I} - \mu_f [\nabla \boldsymbol{u} + \nabla \boldsymbol{u}^T - \tfrac{2}{3}(\nabla \cdot \boldsymbol{u}) \boldsymbol{I}]; \tag{7}$$

(5) then represents a drag force proportional to the difference between the local average velocities and the factor β would be expected to depend on ϕ. For this we adopt the following form, corresponding to the well-known Richardson–Zaki (1954) correlation for sedimentation velocity:

$$\beta = \frac{(\rho_s - \rho_f) g}{v_t} \frac{\phi}{(1-\phi)^{n-1}}, \tag{8}$$

where n depends on the Reynolds number for an isolated particle falling at its terminal velocity v_t. p_f and μ_f are taken to be the local average value of the fluid pressure and the viscosity of the pure fluid, respectively, while p_s and μ_s are assumed to be monotone increasing functions of ϕ which vanish when $\phi = 0$ and increase without bound as $\phi \to \phi_p$, where ϕ_p is the volume fraction of solids at random close packing of the particles. It can be argued that p_s should depend additionally on the relative velocity $|\boldsymbol{u} - \boldsymbol{v}|$, or that p_s and μ_s should depend additionally on the 'particle temperature', or mean square value of the fluctuation of particle velocities about the local average. However, a dependence on ϕ alone, of the nature specified above, is enough to account for a transition from unstable to stable behaviour as ϕ is increased, and to establish a finite length scale for the dominant perturbation at each value of ϕ for which the suspension is unstable. Various specific functional forms have been proposed; the ones adopted here are

$$p_s = P\phi^3 \exp\left(\frac{r\phi}{\phi_p - \phi}\right) \tag{9}$$

and
$$\mu_s = \frac{M\phi}{1 - (\phi/\phi_p)^{1/3}}. \tag{10}$$

Equation (9) is chosen to match an *ad hoc* form used by Hernandez & Jimenez (1991) in calculating bubble development; it contains two constants, P and r, which permit the magnitude and slope of p_s, and hence the critical volume fraction for limiting stability, to be adjusted. The dependence of μ_s on ϕ, given by (10), has a behaviour similar to that of (9). The choice of a value for the parameter M permits the length scale of the

dominant instability to be adjusted. Expressions other than these have been proposed. For example, Harris & Crighton (1994) use the simple form $p_s = P\phi/(\phi_p - \phi)$, while B. Glasser (1994, personal communication) has investigated bifurcation properties of solutions using a constant value for μ_s, in addition to other forms.

If we had been interested only in gas-fluidized beds we could have gone further and introduced approximations associated with the smallness of the density and viscosity of a typical gas, when equations (3) and (4) above would reduce to

$$\rho_s \phi \frac{\mathrm{D}_s \boldsymbol{v}}{\mathrm{D}t} = -\nabla\cdot(\boldsymbol{E}_s + p_f \boldsymbol{I}) + \rho_s \phi \boldsymbol{g}, \tag{11}$$

$$\beta(\boldsymbol{u} - \boldsymbol{v}) = -\nabla p_f. \tag{12}$$

The tensor $\boldsymbol{E}_s$ then represents momentum transfer by particle velocity fluctuations and forces transmitted between particles at points of direct contact, and the proper form for the equations is less uncertain. However, since we wish to simulate both gas- and liquid-fluidized suspensions, the more elaborate forms (3) and (4) should be retained.

As remarked earlier, even these forms are oversimplified, sometimes by assumptions that could easily be improved. For example, the linear expression (5) for the dependence of drag force on the relative velocity of fluid and particles is appropriate only if the Reynolds number, based on this velocity and the particle diameter, is sufficiently small. In our solutions for the gas-fluidized bed this Reynolds number is typically of the order of unity, which is at the upper bound for the linear relation to be a reasonable approximation. In the solutions for the liquid-fluidized bed, on the other hand, Reynolds numbers a decimal order of magnitude larger than this are typical and the linear form should be replaced by something more elaborate. Though this could be done without difficulty, since empirical expressions for the drag force are available in this higher range of Reynolds numbers, we have chosen to retain the simple linear form appropriate for the gas-fluidized case. Anticipating our results, this allows us to show that the distinction between bubbling and non-bubbling behaviour is not a result of differing algebraic forms for the drag force in the two cases. Similar remarks apply to virtual mass effects. These are negligible for the gas-fluidized system, but might be expected to be significant for liquid fluidization. Nevertheless, even though we have omitted them in both cases, we are still able to account for the difference in behaviour.

3. Method of solution

Equations (1)–(4) have trivial solutions representing uniform fluidized beds of infinite extent, namely

$$\phi = \phi_0; \quad \boldsymbol{v} = 0; \quad \boldsymbol{u} = \boldsymbol{i}u_0 = \boldsymbol{i}v_t(1-\phi_0)^{n-1}; \quad \nabla p_f = [\rho_s \phi + \rho_f(1-\phi)]\boldsymbol{g},$$

where $\boldsymbol{i}$ is the unit vector in the upward vertical direction. When ϕ_0 is smaller than some critical value these solutions are linearly unstable to small spatially periodic disturbances. The fastest growing disturbance is an upward travelling wave, of the form $\exp(\sigma_r t)\exp[\mathrm{i}(ky - \sigma_i t)]$, whose wavefronts are horizontal planes. The limiting value of ϕ_0 for stability and the wavelength, growth rate, and velocity of propagation of the dominant wave, for any given value of $\phi < \phi_0$, all depend on the parameters appearing in (3)–(10). A non-zero value of P is needed if there are to be any conditions under which a uniform bed is stable, and a non-zero value of M is needed if there is to be a bounded value of the wavenumber for which the disturbance grows fastest, in

any given unstable bed. The linear stability theory of the unbounded uniform bed has been described exhaustively in the literature (Jackson 1963*a*; Murray 1965; Pigford & Baron 1965; Anderson & Jackson 1968; Garg & Pritchett, 1975; Mutsers & Rietema 1977; Liu 1982; Foscolo & Gibilaro 1984; Batchelor 1988), with much discussion of the physical origin of the stabilizing pressure term p_s.

In this work we shall avoid the computational complications which accompany a bounded bed by restricting attention to spatially periodic structures, and their growth and movement in time. However, we shall not limit considerations to small perturbations of a uniform state, but will generate the solutions by direct numerical integration of the full nonlinear equations of motion. The integration will always start from a small perturbation of a known steady state (for example, the uniform bed) so that the initial development of the disturbance away from the steady state can be predicted from the eigensolutions of the problem generated by linearization about the base state. When the base state is the uniform bed these can be found analytically; in other cases it will be necessary to compute them numerically. By starting in this way with the volume fraction and velocity fields in the correct relative phases, as determined from a linearized problem, we circumvent difficulties arising from stiffness introduced by the shortness of the typical relaxation time for the velocity difference $\boldsymbol{u}-\boldsymbol{v}$.

To be specific, we seek solutions in a rectangular spatial domain of vertical height L_y and horizontal width L_x. The solutions will be constrained to be periodic with period L_y in the y-direction (except for the pressure), and to be symmetric about the vertical median line ($x = 0$) and periodic with period L_x in the x-direction. Explicitly, these conditions are

y-periodicity:

$$\phi(x,0) = \phi(x,L_y); \quad \boldsymbol{u}(x,0) = \boldsymbol{u}(x,L_y); \quad \boldsymbol{v}(x,0) = \boldsymbol{v}(x,L_y); \quad p(x,0) = p(x,L_y) + \Delta p; \tag{13}$$

symmetry and x-periodicity:

$$u_x = v_x = \frac{\partial \phi}{\partial x} = \frac{\partial u_y}{\partial x} = \frac{\partial v_y}{\partial x} = 0 \quad \text{at} \quad x = 0, L_x/2. \tag{14}$$

Note that conditions (14) suppress any solutions in the form of oblique travelling waves. Because of symmetry about the median line the solution can be confined to the half-rectangle, and no conditions are needed at $x = -L_x/2$. In (13) Δp denotes the change in pressure over the height of the rectangle. In the uniform base state, or in the presence of any fully developed travelling wave, this balances the weight of the material in the rectangle. In general, its value must be adjusted to ensure that the average vertical solids flux vanishes in the laboratory reference frame, thereby eliminating the inherent translational ambiguity of the problem. These boundary conditions automatically ensure that the total volume of each phase within the rectangle remains constant; in other words, the mean volume fraction of solids does not change with time.

The discretization is performed using a Galerkin finite element scheme. The rectangular half-cell is divided into a grid of rectangular elements, and within each element the dependent variables are approximated by polynomials. For the fluid pressure bilinear functions of the coordinates within each element are used, and for the remaining variables biquadratic functions. Higher precision can be sought by increasing the order of the polynomial approximating functions, or by decreasing the size and, correspondingly, increasing the number of the elements We have adopted the second alternative to test the adequacy of our discretization. In principle the elements

	Air	Water
ρ_s	2.2 g cm^{-3}	2.2 g cm^{-3}
ρ_f	0.0013 g cm^{-3}	1 g cm^{-3}
μ	0.000181 g cm^{-1} s^{-1}	0.01 g cm^{-1} s^{-1}
a	100 μm	0.5 mm
v_t	142 cm s^{-1}	14.3 cm s^{-1}
n	4.25	3.65
ϕ_p	0.65	0.65
P (eq. (9))	10.78 dyn cm^{-2}	0.266 dyn cm^{-2}
r (eq. (9))	0.3	0.3
M (eq. (10))	0.571 g cm^{-1} s	0.571 g cm^{-1} s

TABLE 1. Properties of the air- and water-fluidized beds

need not all be of the same size, and this feature could be used to advantage in handling steep spatial gradients. However, elements of uniform size were used throughout the work reported here. The solution is advanced in time using an implicit one-step Euler method.

For the purpose of the computations it is clearly desirable to scale lengths in terms of the specified size of the periodic cell. To make the equations dimensionless two other quantities are needed, for example a density and a velocity. In view of the dominance of the solids mass in a gas-fluidized bed it is appropriate to choose ρ_s as the density but, as we shall see, there are several candidates for the scaling velocity. In the computations the terminal velocity v_t is used, so that dimensionless variables are defined as follows:

$$x^* = \frac{x}{L_x}; \quad y^* = \frac{y}{L_y}; \quad t^* = \frac{tv_t}{L_y}; \quad (\boldsymbol{u}^*, \boldsymbol{v}^*) = \frac{(\boldsymbol{u}, \boldsymbol{v})}{v_t}; \quad \boldsymbol{E}_f^*, \boldsymbol{E}_s^* = \frac{(\boldsymbol{E}_f, \boldsymbol{E}_s)}{\rho_s v_t^2},$$

which introduces the dimensionless groups

$$\rho_s v_t L_y / M, \quad P/\rho_s v_t^2, \quad v_t^2/gL_y, \quad \rho_f/\rho_s, \quad \mu_f/M$$

in addition to the dimensionless parameters r and ϕ_p. However, it must be emphasized that this is not claimed to be a physically significant scaling.

The question of a physically appropriate scaling for the problem of disturbance propagation in a fluidized bed is a difficult one. As noted above, the fastest growing small disturbance in such a bed is a plane wave with horizontal wavefronts, propagating in the upward vertical direction. Its wavelength, speed of growth and velocity all depend on ϕ_0, and the wavelength and reciprocal of the speed of growth clearly provide the physically relevant length and time scales. In the computations the cell height L_y should be of the order of this wavelength. It would, therefore, be desirable to relate these quantities to the basic properties of the particles and the fluid for the two systems studied here, as listed in table 1. However, stability theories relate the parameters of the propagating disturbances only to effective mechanical properties of the uniform unperturbed state. As emphasized by Batchelor (1988) our physical understanding of the micromechanics of suspensions is not yet adequate to link these, in turn, to the bed expansion and the physical properties of the fluid and the particles. At best, therefore, we must settle for scalings related to effective properties of the uniform bed which are, in principle, independently measurable.

With the expression (9) or other analytical forms for p_s there is a further difficulty. In this work we study two systems, namely a bed of 200 μm diameter glass beads fluidized by air at ambient conditions and a bed of 1 mm diameter glass beads fluidized

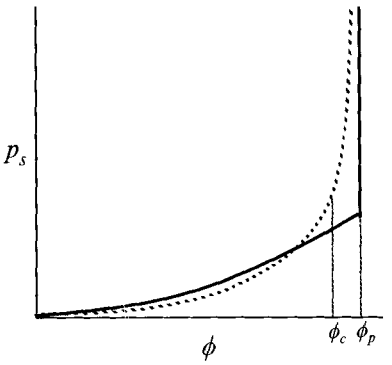

FIGURE 1. Dependence of p_s on ϕ assumed in this work (broken curve) compared with a more realistic form of this dependence (continuous curve).

by water. Their relevant physical properties are listed in table 1. Both these systems would be expected to have about the same solids volume fraction at minimum fluidization, and in both cases the onset of instability would be expected immediately beyond minimum fluidization. It would, therefore, be appropriate to compare the propagation of disturbances in each of the two suspensions at a common value of the solids volume fraction, slightly smaller than that at minimum fluidization. However, with the expression for p_s used here, and sketched as the broken curve in figure 1, there is no phenomenon of minimum fluidization. Because p_s is represented as increasing without bound asymptotically as $\phi \to \phi_p$ the bed begins to expand reversibly as soon as the fluid velocity increases from zero. This smooth expansion is interrupted only at the critical volume fraction ϕ_c where the uniform suspension becomes unstable. The actual behaviour of beds like those treated here is represented better by a form for p_s indicated by the solid curve sketched in figure 1. Then both p_s and its derivative with respect to ϕ remain bounded when $\phi \to \phi_p$, and their values are such that the uniform bed is unstable for all $\phi < \phi_p$. For all larger values of p_s, ϕ retains the constant value ϕ_p, reflecting the incompressibility of a random packing of hard spheres. With this form for p_s expansion of the bed occurs only when the fluid velocity reaches a value where the drag force balances the weight of the particles (the condition of minimum fluidization) and the expanded bed immediately becomes unstable. Since the form for p_s given by (9) predicts a transition from stability to instability at some critical volume fraction ϕ_c (smaller than ϕ_p) but no condition of minimum fluidization, the closest analogue of a real dense fluidized bed we can find, with this form for p_s, is a spatially uniform suspension with solids volume fraction slightly smaller than ϕ_c. This is the base state chosen for the present work and its volume fraction will be denoted by ϕ_0. However, this choice introduces a further difficulty into the selection of a scaling length, since it is found that the wavelength of the fastest growing small perturbation increases without bound as $\phi_0 \to \phi_c$. Thus the scaling length depends in a very sensitive manner on the choice of ϕ_0 and it increases without bound as $\phi_0 \to \phi_c$. Clearly then, in these circumstances there is no question of identifying a unique, characteristic length scale related to the properties of the particles and the fluid. Instead we must be content with the scale set by the wavelength of the dominant disturbance itself in the particular base state we select. Fortunately, to relate this wavelength, and the corresponding rate of growth, to the bed expansion and other effective properties of the unperturbed bed requires only the solution of a quadratic equation, so although these scaling variables cannot be written down as simple multiples or ratios of the mechanical properties of

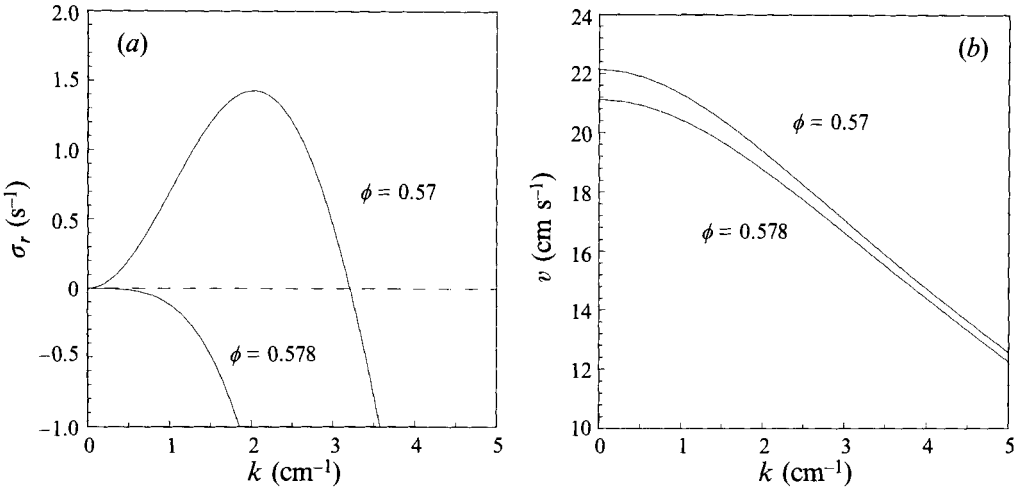

FIGURE 2. Linear stability results for one-dimensional waves in an air-fluidized bed of 200 μm glass beads: (*a*) growth rate σ_r, (*b*) wave speed v, as functions of wavenumber k.

the uniform bed, they are easily calculated from these properties. These considerations are relevant to the scaling of one-dimensional disturbances. Scaling for disturbances with two-dimensional structure will be discussed further in §8.

In the present work the constant r in equation (9) is given the same value for both the gas- and liquid-fluidized beds, and so is the constant M in equation (10) (see table 1). In the light of the above discussion, however, for each bed the value of P is selected to make $\phi_c = 0.578$, which is a reasonable representation of the volume fraction at minimum fluidization for particles of the type considered. As can be seen from table 1 the required value of P is much smaller for the water-fluidized bed than the gas-fluidized bed, reflecting the relative ease with which this bed can be stabilized. A value $\phi_0 = 0.57$ is then selected for the base states, in both the gas- and liquid-fluidized beds. This lies just on the unstable side of the stability limit, and the value of $\mu_s(\phi_0)$ is 7.6 g cm^{-1} s^{-1}. Though large, this is of the same order of magnitude as reported measurements of viscosity for dense fluidized suspensions.

Figures 2(*a*) and 2(*b*) show the growth, σ_r, and the velocity of propagation, v, of small perturbations, sinusoidal in y, in the uniform gas-fluidized bed (found explicitly by linearization of the equations) as functions of wavenumber, k, both at the expansion corresponding to limiting stability, and at ϕ_0. At bed expansion ϕ_0 the growth is most rapid at a wavelength of about 3.14 cm, so this sets the length scale for the gas-fluidized bed. Figures 3(*a*) and 3(*b*) give the corresponding information for the water-fluidized bed, and here the wavelength of the dominant disturbance is 1.86 cm. All the properties of the dominant small disturbance are listed for each bed in table 2, where other properties of the base state, such as the fluidization velocity u_0, the continuity wave speed V, and the speeds of the upward and downward propagating dynamic waves, c_u and c_d, are also quoted. (For definitions of the continuity and dynamic wave velocities see, for example, Liu 1982.) Both the growth rates and the speeds of propagation in the liquid-fluidized bed are seen to be smaller than those in the gas-fluidized bed by at least a decimal order of magnitude.

Note that there is a critical value of the wavenumber for each bed, above which the uniform bed is stable, and this increases as the bed is expanded. As a result, computational difficulties might be expected whenever these is an extended region of

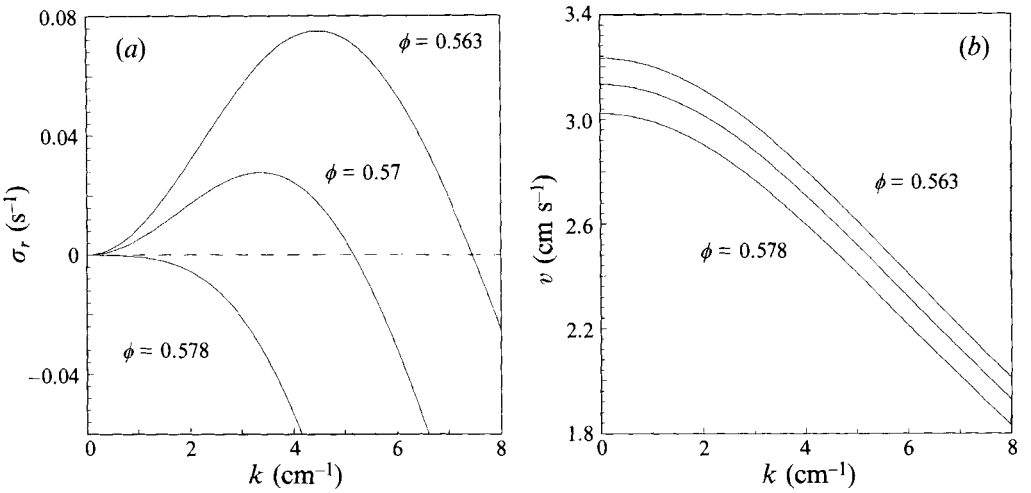

FIGURE 3. Linear stability results for one-dimensional waves in a water-fluidized bed of 1 mm glass beads: (*a*) growth rate σ_r, (*b*) wave speed v, as functions of wavenumber k.

	Gas	Liquid
Solids volume fraction, ϕ_0	0.57	0.57
Fluidization velocity, u_0	9.14 cm s^{-1}	1.53 cm s^{-1}
Continuity wave speed, V	22.15 cm s^{-1}	3.18 cm s^{-1}
Upward dynamic wave speed, c_u	16.57 cm s^{-1}	2.07 cm s^{-1}
Downward dynamic wave speed, c_d	16.55 cm s^{-1}	1.02 cm s^{-1}
Wavelength of dominant mode, λ^m	3.14 cm	1.86 cm
Speed of dominant mode, v^m	19.4 cm s^{-1}	2.82 cm s^{-1}
Growth time of dominant mode, $1/\sigma_r^m$	0.689 s	36.1 s

TABLE 2. Properties of the unperturbed uniform beds

suspension whose concentration is so low that waves on the length scale of the computational elements become unstable. Numerical ripple would then be expected to grow and interfere with the solution. This difficulty might be mitigated with other algebraic forms for the dependence of p_s on ϕ, such as that used by Harris & Crighton (1994), which predict a restabilization of the bed at sufficiently high expansion.

4. One-dimensional structures

We now address the propagation and growth of one-dimensional waves with horizontal plane wavefronts. The initial stages of motion can then be found analytically by linearization about the uniform bed, introducing a perturbation of the form $\exp(\sigma^* t^* + \mathrm{i}k^* y^*)$ in terms of the dimensionless variables used in the computations, where $\sigma^* = \sigma_r^* - \mathrm{i}\sigma_i^*$. This is valuable in a number of ways for the subsequent numerical integration. First, the adequacy of the subdivision of the computational domain into elements can be tested by comparing the explicit expressions for the eigenvalues with the corresponding eigenvalues of the computational algorithm. The element size is decreased until the latter converge on the former to acceptable accuracy. Secondly, the explicit solution of the linearized problem provides initial conditions for the numerical integration, with the concentration, pressure and velocity fields close to the proper

phase relation with each other, eliminating the potential problem of following rapid transients as this relation is established. Thirdly, the short-time solutions, generated by integration forward in time, can be compared with the known solutions from linearization to check that the time step used in the numerical integration is short enough, at least initially.

If it was intended to confine attention entirely to one-dimensional motions it would be efficient to write a separate, and much simpler, code to generate them. However, the most interesting results are found in two dimensions, and in the way initially one-dimensional motions develop into the second dimension when the constraint of one-dimensionality is lifted, so we have used the full two-dimensional algorithm throughout, constraining the motion to be one-dimensional, when required, by making the cell narrow in the lateral direction and spanning its half-width with a single element. Then, for the gas-fluidized bed and a cell with $L_y = 3.14$ cm (the wavelength λ^m of the dominant linear mode) table 3 illustrates how the three eigenvalues of the computational algorithm with the (algebraically) largest real parts converge toward the corresponding explicitly determined eigenvalues, as the number of intervals into which the cell is divided in the vertical direction increases. Convergence is seen to be rapid as the grid is refined. With twenty intervals the real and imaginary parts of the dominant computed and explicitly determined eigenvalue differ by no more than one in the fourth significant figure. The precision of the computed values of the two more-stable eigenvalues is not as high, but is never worse than one part in a hundred.

The length of the time step needed to maintain adequate accuracy can be increased substantially by carrying out the integration in a reference frame that is moving at a velocity close to that of the propagating wave. This velocity changes, of course, as the wave grows, so the speed of the reference frame is also changed, from time to time, whenever it differs significantly from that of the wave. As we shall see, the waveform eventually develops a pronounced asymmetry and may change shape quite quickly as it rises through the bed. The objective is then to match the speed of the reference frame to the speed of rise of the steepest part of the wave profile.

Computations of one-dimensional waves similar to those described here have previously been reported by Needham & Merkin (1986), but their results were restricted to gas-fluidized beds.

It was noted in the Introduction that linear stability theory indicates only quantitative differences between gas- and liquid-fluidized beds, both growth rates and speeds of propagation being much larger in the former. Since we seek qualitative differences in behaviour, in presenting the results it is convenient to suppress the merely quantitative differences by scaling times in terms of the growth time $(1/\sigma_r^m)$ for the fastest growing small perturbation. Lengths are scaled in terms of the wavelength λ^m of this perturbation, and velocities will be quoted as multiples of the continuity wave velocity V, given in table 2 for each system. (Later it will be useful to express them alternatively as multiples of the fluidization velocity u_0.) Distinguishing these dimensionless forms by tildes, we have

$$\tilde{t} = t\sigma_r^m, \quad \tilde{L}_y = L_y/\lambda^m, \quad \tilde{v} = v/V.$$

For the gas-fluidized bed figure 4(*a*) illustrates the computed development of an initially small, sinusoidal perturbation with the wavelength λ^m (3.14 cm). Profiles of the solids volume fraction are shown at a sequence of values of $\tilde{t}$. At $\tilde{t} = 2.9$ the wave is essentially fully developed and thereafter it propagates without significant change in form. (In all the one-dimensional waves illustrated below the final wave profiles are also fully developed.) The relative positions of the profiles give no indication of the

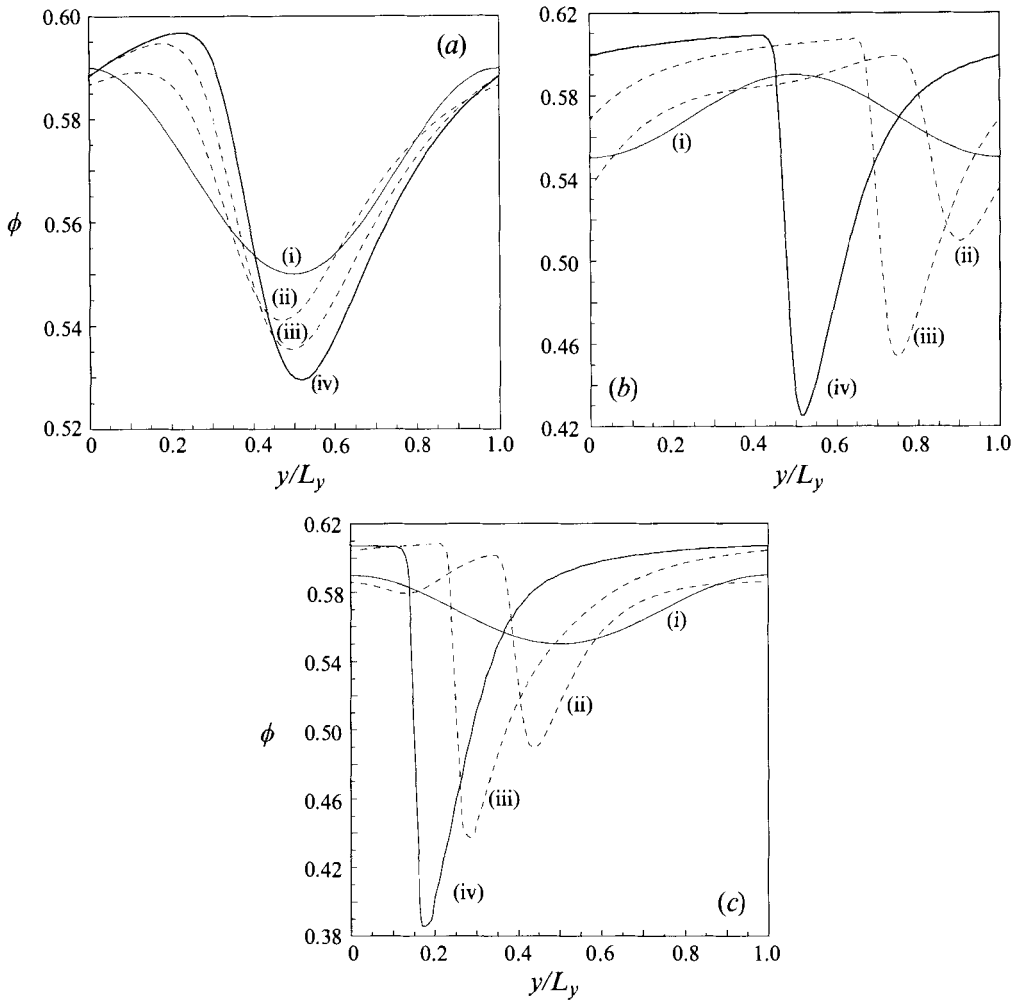

FIGURE 4. Development of one-dimensional waves in the air-fluidized bed. (*a*) The fastest growing wave $\tilde{L}_y = 1$: (i) $\tilde{t} = 0$, (ii) $\tilde{t} = 0.16$, (iii) $\tilde{t} = 0.80$, (iv) $\tilde{t} = 2.9$; initial wave speed: $\tilde{v} = 0.876$, final wave speed: $\tilde{v} = 0.844$. (*b*) $\tilde{L}_y = 2$: (i) $\tilde{t} = 0$, (ii) $\tilde{t} = 0.58$, (iii) $\tilde{t} = 1.9$, (iv) $\tilde{t} = 3.2$; initial wave speed: $\tilde{v} = 0.966$, final wave speed: $\tilde{v} = 0.862$. (*c*) $\tilde{L}_y = 3$: (i) $\tilde{t} = 0$, (ii) $\tilde{t} = 0.97$, (iii) $\tilde{t} = 2.58$, (iv) $\tilde{t} = 2.85$; initial wave speed: $\tilde{v} = 0.975$, final wave speed: $\tilde{v} = 0.889$.

No. of intervals in L_y	Eigenvalue 1	Eigenvalue 2	Eigenvalue 3
5	0.03407–0.8255i	—	—
10	0.03179–0.8568i	−0.06276–1.2703i	−0.29726–1.1890i
15	0.03209–0.8579i	−0.05475–1.3000i	−0.25217–1.3771i
20	0.03212–0.8581i	−0.05354–1.3037i	−0.24496–1.4022i
Analytical	0.03213–0.8581i	−0.05312–1.3049i	−0.24249–1.4102i

TABLE 3. Convergence of computed eigenvalues for gas fluidized bed, $L_y = \pi$ cm

upward motion of the wave, since the frame of reference is adjusted as described above. However, as noted in the caption, the wave decelerates from an initial dimensionless speed $\tilde{v}$ (relative to the rest frame) of 0.876, when the amplitude is small, to a final speed $\tilde{v} = 0.844$. The profile also becomes asymmetric, assuming the form of periodic plugs

of high-density material with a sharper upper surface and a more diffuse lower surface. This asymmetry has previously been predicted, on different grounds, by Fanucci *et al.* (1979), Ganser & Drew (1990), Dankworth & Sundaresan (1991) and Göz (1992). The same fully developed wave can be reached from other initial conditions; for example, if the amplitude of the initial sine wave perturbation is larger than that of the fully developed wave, it is found to decay to the same final profile.

The integration can, of course, be started from small sinusoidal perturbations of the uniform bed with wavelengths other than λ^m, and figures 4(*b*) and 4(*c*) show the results for wavelengths $2\lambda^m$ and $3\lambda^m$, respectively. The results are qualitatively similar to those seen in figure 4(*a*). Both the initial and final wave speeds, and the time needed to reach the fully developed waveform, increase a little as the wavelength is increased, but it is important to note that the order of magnitude of the elapsed time remains the same in all cases. With increase in wavelength the most striking change is the marked increase in depth of the band of low concentration. The spatial width of this band remains approximately the same in all three cases; as the wavelength is increased the extra material, no longer accommodated in the band of low density, is taken up by a dense bed with solids volume fraction 0.6 or larger, which separates the bands of low density. These two observations are not unrelated. Since the mean volume fraction remains 0.57 in all cases, and the volume fraction in the dense regions remains near 0.6, the decrease in concentration in the band of low concentration with increasing wavelength is an immediate consequence of the fact that its width does not change significantly.

Figure 4(*c*) illustrates very clearly the mechanism of propagation of these waves. They consist of a sequence of plugs with high particle concentration. The unsupported lower surface of each plug (the left side in the figure) is unstable, and particles rain down from it, accelerating under gravity so that their concentration decreases on moving down. They then decelerate suddenly as they meet the sharp upper boundary of the plug below. This transfer of the particles from each plug to its neighbour below is responsible for the upward motion of the whole concentration pattern. The phenomenon is quite familiar in practice from observations of gas-fluidized beds in long narrow tubes.

The above results are consistent with those of Needham & Merkin (1986). Our unperturbed bed is 'dense', in the sense of those authors (i.e. $1-\phi_0 < E^*$, in their notation) and we see a pattern of extended plugs of high particle concentration separated by narrower bands of low concentration, in agreement with their results. However, their computed solutions are all of quite small amplitude and, correspondingly, short wavelength. The marked asymmetry of our results is not seen in theirs. This may be a consequence of their assumption that $p_s \propto \phi$, or may simply be a consequence of the small amplitudes of their waves.

Figure 5(*a–c*) shows the development of one-dimensional waves from small initial perturbations of the water-fluidized bed. The wavelength λ^m (1.86 cm), shown in figure 5(*a*), corresponds to the fastest growing small perturbation, while figures 5(*b*) and 5(*c*) exhibit the results for double and treble this wavelength, respectively. Thus, figure 5 is the analogue, for the water-fluidized bed, of figure 4, and the results, in terms of the scaled variables, are seen to be similar. The time required to reach the fully developed waveform in all cases lie between two and four times the growth time for the fastest growing small perturbation. The amplitudes achieved by the fully developed waves are similar at corresponding multiples of λ^m; indeed, for wavelength $3\lambda^m$ the amplitude is larger in the water-fluidized bed. In all cases the velocity of propagation is of the same order as the continuity wave velocity, and it changes little as the disturbance grows. (In most cases there is a small decrease, while the small increase recorded in the last two

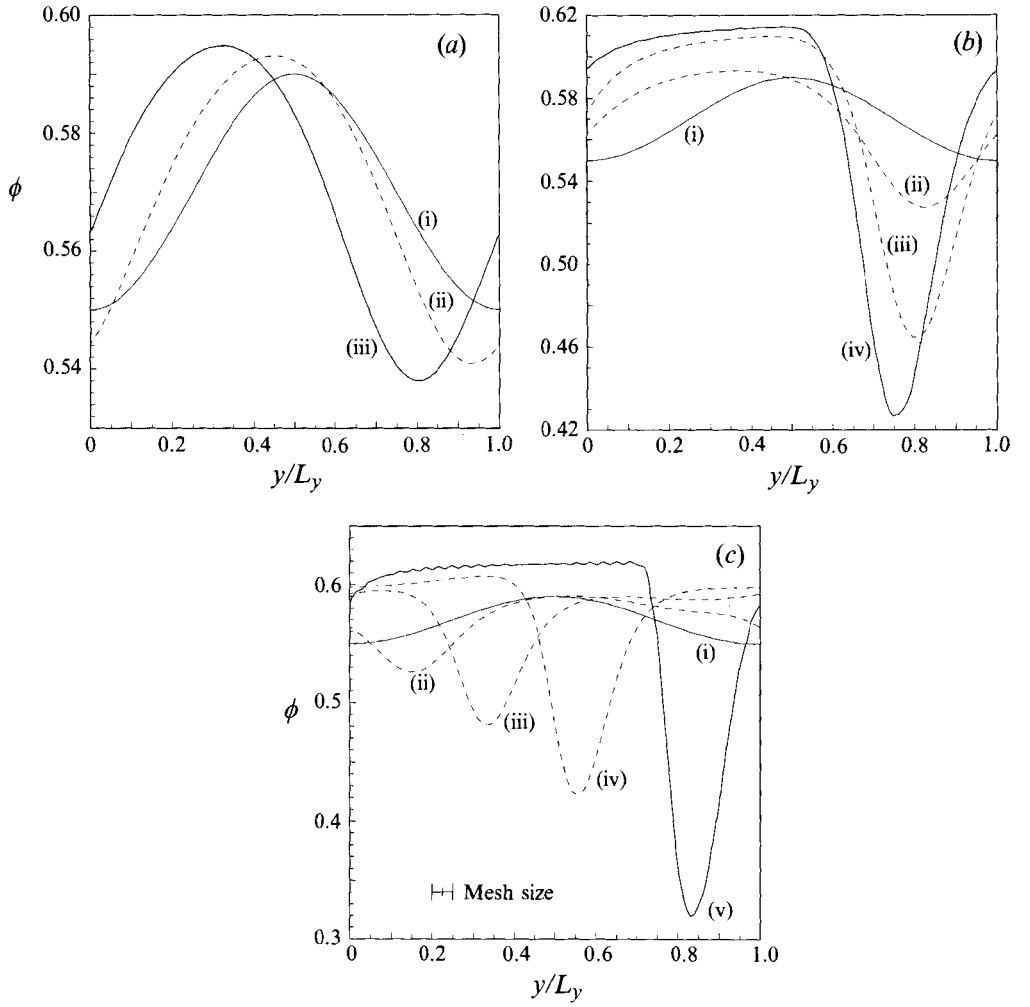

FIGURE 5. Development of one-dimensional waves in the water-fluidized bed. (*a*) The fastest growing wave $\tilde{L}_y = 1$. (i) $\tilde{t} = 0$, (ii) $\tilde{t} = 0.72$, (iii) $\tilde{t} = 1.8$; initial wave speed: $\tilde{v} = 0.887$, final wave speed: $\tilde{v} = 0.884$. (*b*) $\tilde{L}_y = 2$. (i) $\tilde{t} = 0$, (ii) $\tilde{t} = 0.72$, (iii) $\tilde{t} = 1.44$, (iv) $\tilde{t} = 2.16$; initial wave speed: $\tilde{v} = 0.959$, final wave speed: $\tilde{v} = 0.969$. (*c*) $\tilde{L}_y = 3$: (i) $\tilde{t} = 0$, (ii) $\tilde{t} = 0.64$, (iii) $\tilde{t} = 1.20$, (iv) $\tilde{t} = 1.52$, (v) $\tilde{t} = 2.16$; initial wave speed: $\tilde{v} = 0.975$, final wave speed: $\tilde{v} = 0.984$.

cases lies within the uncertainty in evaluating this velocity.) The only noticeable qualitative difference between the gas- and liquid-fluidized systems lies in the asymmetry of the particle concentration profiles, which is less marked for the liquid-fluidized bed. There is no qualitative distinction in behaviour that could explain why bubbles are seen, in practice, in the gas-fluidized case, but not in the liquid-fluidized case. Thus, this question is not resolved by replacing a linear small-amplitude approximation by the full nonlinear equations, if attention remains confined to one-dimensional motions.

The fully developed waves described so far have all been grown from small perturbations of an initially unstable uniform fluidized bed. It is interesting to note that the same sort of wave can also be grown from a stable uniform bed, provided the initial perturbation is large enough and the bed is near enough to the stability limit. For example, we have found that sufficiently large sinusoidal perturbations of the gas-

fluidized bed with $\phi_0 = 0.58$, just on the stable side of the critical volume fraction, will grow into fully developed waves similar in every respect to those described above. This coexistence of a stable state of uniform fluidization and a large-amplitude travelling wave solution is a consequence of the fact that the bifurcation at $\phi = 0.578$ is subcritical in this case (B. Glasser 1994, personal communication).

5. Stability of the fully developed one-dimensional waves

When viewed from a frame of reference moving at its own speed, a fully developed wave is a time-independent solution of the equations of motion. Its stability can be investigated either by retaining the constraint of one-dimensionality, or by viewing it as a degenerate case of a two-dimensional solution and questioning its stability to two-dimensional perturbations. Since the base state is now a numerically generated non-uniform solution of the equations of motion the eigenvalues cannot be found analytically, but they can be approximated as the eigenvalues of the numerical algorithm. These can then be computed, for partitions of the periodic cell into successively increasing numbers of elements, until they converge. In this way each of the fully developed waves described in the previous section is found to have only eigenvalues with negative real parts, provided the perturbed wave is constrained to remain one-dimensional and to retain the same minimum spatial period as the fully developed wave itself. With these constraints, therefore, all the fully developed, one-dimensional waves reported here are stable.

However, each fully developed solution is also periodic with any integer multiple of its shortest period, so its stability can also be investigated under the less restrictive constraint that the perturbed wave shall remain periodic with one of these longer periods. As an example of this consider the fully developed wave of wavelength λ^m in the air-fluidized bed, shown in figure 4(*a*). When this is exposed to perturbations of period $2\lambda^m$ the leading eigenvalues are found to be a complex-conjugate pair in the right half-plane. After perturbing the fully developed wave by adding a small multiple of the corresponding eigenfunction, numerical integration generates the sequence of concentration profiles shown in figure 6. It is seen that one period of the fully developed wave of wavelength λ^m grows at the expense of the other, finally converging to a single period of the fully developed wave of wavelength $2\lambda^m$ that was shown previously in figure 4(*b*). The total elapsed time for this process is rather longer than the times seen earlier for growth of the waves from small perturbations of the uniform bed.

Similar results are found for other one-dimensional waves, in both the gas- and the liquid-fluidized beds. Each wave is stable to perturbations constrained to its smallest period, but unstable when the constraint is relaxed to a multiple of this period. When this multiple is twice the smallest period, adjacent bands of low particle concentration coalesce, leading to the fully developed wave with wavelength twice that of the original wave. It is not clear how long this pattern of behaviour persists as the wavelength of the wave is increased. We have indications that, for very long waves, behaviour of the type just described may not occur. Instead the pattern of concentration appears to break up and then remain time-dependent without settling into any regular pattern. This may be related to the existence of an upper bound on the wavelength for stable one-dimensional waves, as predicted by Needham & Merkin (1986).

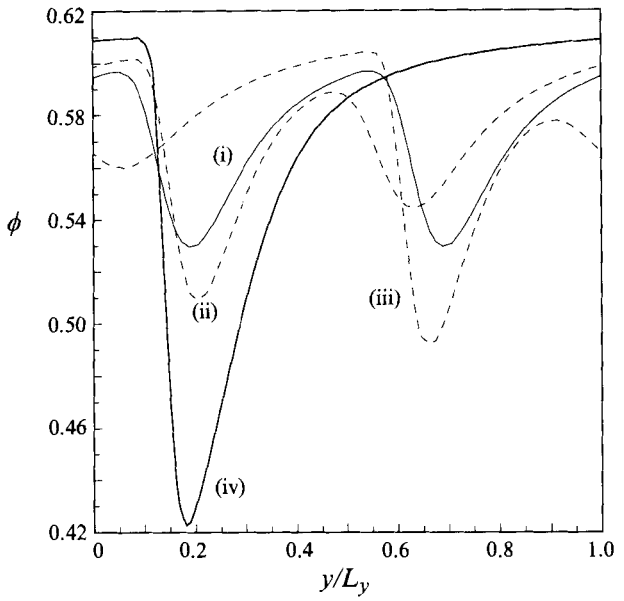

FIGURE 6. Coalescence of adjacent waves of the fully developed one-dimensional wavetrain of wavelength λ_m in the air-fluidized bed, when constrained to cell with $L_y = 2\lambda_m$. (i) $\tilde{t} = 0$, (ii) $\tilde{t} = 3.19$, (iii) $\tilde{t} = 5.81$, (iv) $\tilde{t} = 9.0$. Final wave speed: $\tilde{v} = 0.862$.

6. Two-dimensional motions in the air-fluidized bed

Linear analyses (Didwania & Homsy 1982; Batchelor & Nitsche 1991; Batchelor 1993) indicate that the one-dimensional waves may be unstable to two-dimensional perturbations. This question can be investigated by increasing the width of the computational cell in the horizontal direction, thus admitting solutions of specified, but not necessarily the same, periodicity in each of the orthogonal spatial directions. For each size of cell the subdivision into elements can then be refined until the eigenvalues with largest real parts converge, and the location of these eigenvalues in the complex plane then determines the stability of the one-dimensional wave to two-dimensional perturbations with the specified spatial periodicities. The width of the cell in the horizontal direction can subsequently be varied to find the value of L_x for which the leading eigenvalue lies furthest to the right in the complex plane, thus identifying the most unstable (or least stable) perturbation. As L_x is increased from zero it is found that an eigenvalue migrates along the real axis into the right half-plane. With further increase in L_x this motion continues, and the leading eigenvalue may be followed by others. All these eigenvalues are real and, if L_x is increased still further, their motion reverses and they retreat. As an example, figure 7 shows the distribution of the computed eigenvalues for the fully developed, one-dimensional wave of wavelength $2\lambda^m$ in the air-fluidized bed, with $L_x = L_y$. The real part of the leading eigenvalue, which is largest with this value of L_x, is positive as noted above, so the one-dimensional wave is unstable to this two-dimensional perturbation. The procedure followed to track the evolution of two-dimensional structure is then the same as that described above for the one-dimensional case. A small multiple of the eigenfunction corresponding to the leading eigenvalue is added to the fully developed one-dimensional solution, then numerical integration starts from this initial condition.

The solids volume fraction thus generated at successively increasing values of the time is depicted in figure 8(*a–d*) by shading on a grey scale, with white representing

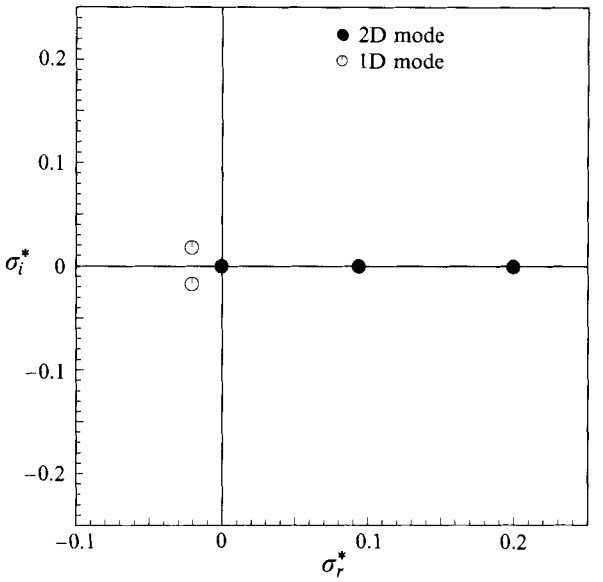

FIGURE 7. Leading eigenvalues for the fully developed one-dimensional wave of wavelength $2\lambda_m$ in the air-fluidized bed, when constrained to a cell with $L_y = L_x = 2\lambda_m$. $(\sigma_r^*, \sigma_i^*) = (\sigma_r, \sigma_i) L_y / v_t$.

$\phi = 0$ and black $\phi = \phi_p = 0.65$. The initial perturbation is seen to distort the band of low particle concentration slightly, so that it is wider in the middle of the cell than at the edges. As time passes this distortion increases, the central part of the pattern begins to move up relative to the part near the edges of the cell, and the concentration of particles decreases further in a compact region situated symmetrically about the centreline of the cell at the apex of the distorted wave. The lowest value reached by the solids volume fraction is $\phi = 0.265$ at the final time. The whole of the development shown in these four panels is complete at $\tilde{t} = 0.90$, so it is comparable in speed with the development of the one-dimensional wave from the uniform bed.

The velocities of both fluid and particles at $\tilde{t} = 0.90$ (seen from a reference frame with upward velocity $\tilde{v}_f = 0.862$) are shown in figure 9, with representation by velocity vectors on the left and instantaneous streamlines on the right. Contours of solids volume fraction are superimposed to relate the velocity fields to the concentration distributions of figure 8. (Some caution is needed in interpretation of this and subsequent similar figures, since the flow pattern is not yet fully developed so streamlines and particle paths do not coincide for either phase.) The most striking feature is the almost closed vortex in the fluid velocity field, centred a little above the point of lowest solids volume fraction, and comparable in size with the largest of the closed volume fraction contours. The particle streamlines bend away from the median line of the cell as they traverse the region of low particle concentration, so the particles tend to move round this region, rather than through it. Consequently the mean density of the suspension on the lateral boundaries of the cell is higher than that of the original uniform bed, while the mean density on the median line is lower. Note that the speed of the frame of reference remains the same as the velocity of rise of the fully developed one-dimensional wave to which the perturbation was applied. There is very little change in the velocity of rise of the particle concentration pattern in the earlier stages of growth, but the compact region of low concentration is beginning to accelerate upward at $\tilde{t} = 0.90$.

For the fully developed one-dimensional wave with $L_y = 3\lambda^m$, shown in figure 4(*c*),

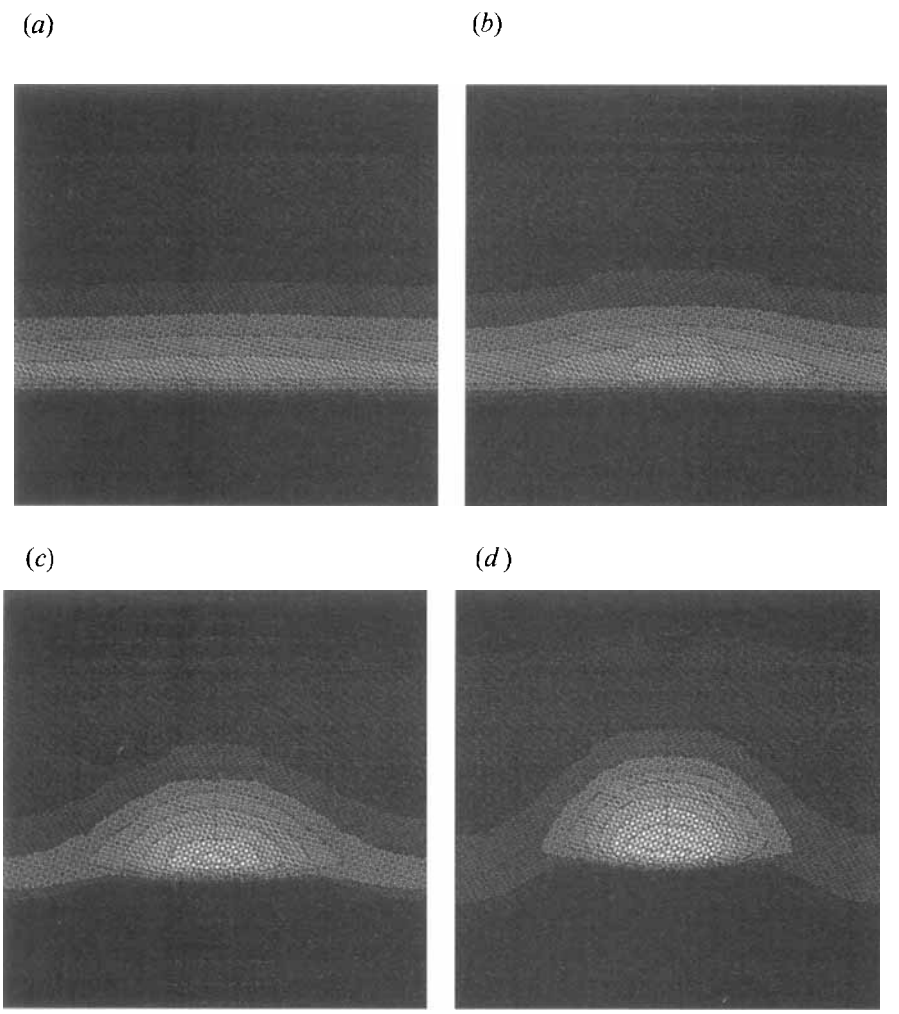

FIGURE 8. Two-dimensional growth of the perturbed fully developed one-dimensional wave of wavelength $2\lambda_m$ in the air-fluidized bed. $L_y = L_x = 2\lambda_m$. 10×40 element mesh. $\Delta t^* = 0.01$. (*a*) $\tilde{t} = 0$, (*b*) $\tilde{t} = 0.45$, (*c*) $\tilde{t} = 0.77$, (*d*) $\tilde{t} = 0.90$.

the real part of the leading eigenvalue is found to be largest when $L_x \approx 2\lambda^m$. With initial conditions corresponding to the fully developed one-dimensional wave, supplemented by a small increment of the eigenfunction belonging to this eigenvalue, the computed solids fraction distributions at successively increasing times are shown in figure 10. The general picture is similar to figure 8, as is the total elapsed time, namely $\tilde{t} = 0.75$. During the computations the speed of the frame of reference is adjusted, from time to time, so that the region of steepest concentration gradient, around the floor of the 'bubble' of low particle concentration, remains approximately at rest in the current frame. The velocity of rise of the one-dimensional wave from which the solution started is $\tilde{v} = 0.888$, while the velocity of the working frame (relative to the rest frame) at $\tilde{t} = 0.75$ is $\tilde{v}_f = 1.14$. At this time the spatial distribution of particle concentration, viewed from the working frame, is changing only slowly, so it can be regarded as rising at this speed without significant change of form, when viewed from the rest frame. Expressed in terms of the fluidization velocity the rise velocity of the concentration pattern is, therefore, $2.76u_0$.

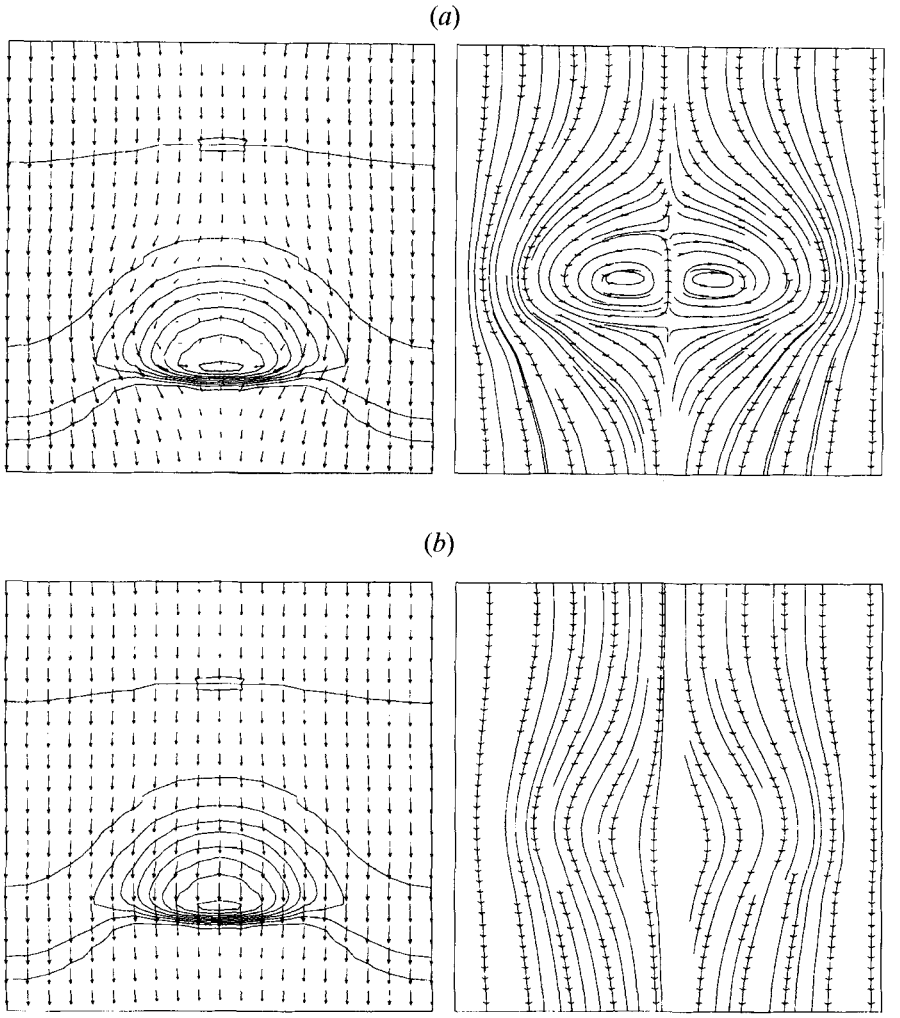

FIGURE 9. Velocity fields for the solution of figure 8 at $\tilde{t} = 0.90$: (*a*) fluid velocity (longest vector = $1.63u_0$); (*b*) solids velocity (longest vector = $3.15u_0$). $\tilde{v}_f = 0.862$ ($v_f = 2.09u_0$).

At $\tilde{t} = 0.75$ the solution bears a strong resemblance to a bubble in a fluidized bed or, rather, one member of an infinite two-dimensional array of bubbles. The lowest particle concentration reached is $\phi = 0.14$, which by no means matches the conventional picture of a bubble completely free of particles. However, the minimum concentration is still decreasing slowly and there is a bound on how low it can go, given the spatial extent of the bubble, imposed by the requirement that the mean volume fraction of solids over the whole cell must retain the starting value of 0.57. (A similar consideration limited the lowest concentration achievable in a one-dimensional wave.) This bound could be lowered by considering an even larger cell, but then computational problems begin to impose a limit. As the solids volume fraction of a uniform bed is decreased the limiting value of the wavenumber, separating stable from unstable behaviour, increases. Eventually the corresponding wavelength becomes shorter than the vertical dimension of the computational elements, and at this point any numerical ripple, on the scale of these elements, will begin to grow. Thus, as noted earlier, we might anticipate numerical difficulties whenever there is an extended region with

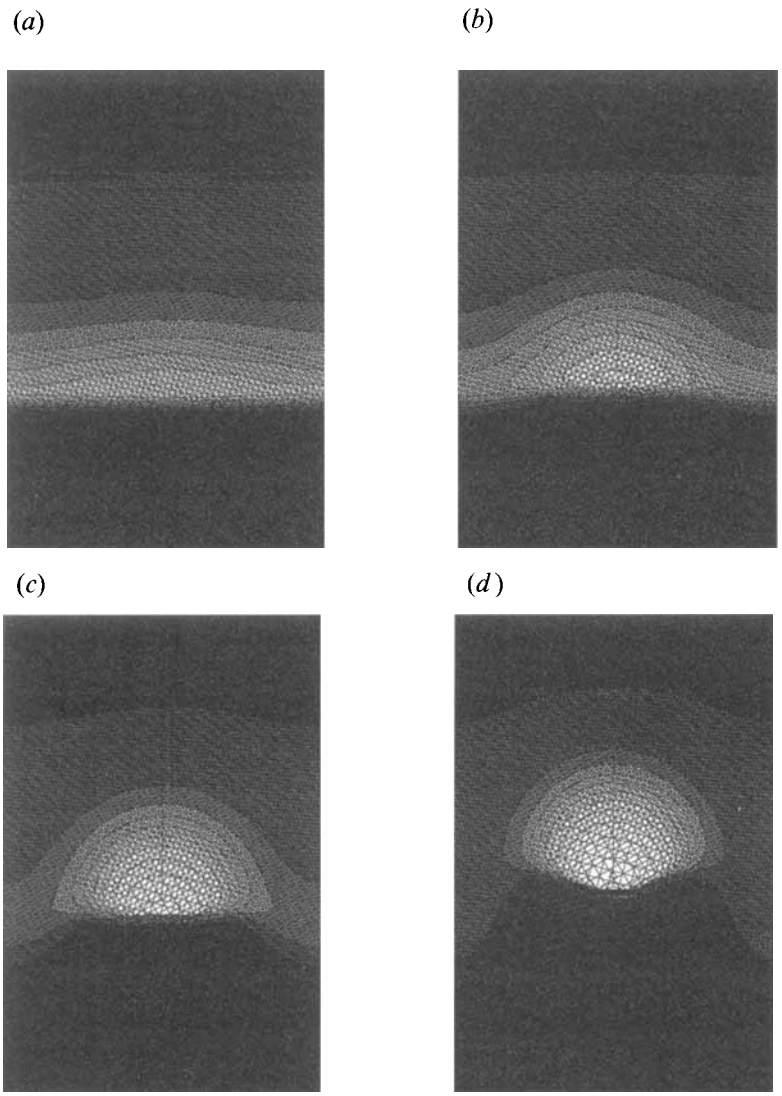

FIGURE 10. Two-dimensional growth of the perturbed fully developed one-dimensional wave of wavelength $3\lambda_m$ in the air-fluidized bed. $L_y = 3\lambda_m$, $L_x = 2\lambda_m$. 20×40 element mesh. $\Delta t^* = 0.01$. (*a*) $\tilde{t} = 0$, (*b*) $\tilde{t} = 0.36$, (*c*) $\tilde{t} = 0.58$, (*d*) $\tilde{t} = 0.75$.

particle concentration so low that ripples on this scale can grow. Of course, this is not an absolute barrier to progress, since the onset of ripples can be delayed by going to a smaller element size, but there are obvious practical limits to this strategy. As remarked earlier, this difficulty could possibly be eliminated by using an algebraic form for the dependence of p_s on ϕ which makes the bed stable at low particle concentrations.

The computed 'bubble' has a diffuse roof, through which the particle concentration increases gradually on moving up into the dense bed, but there is a relatively sharply defined floor. (These features mirror corresponding observations for the one-dimensional wave.) The presence of a mantle of reduced particle concentration above the bubble was first predicted by one of the present authors (Jackson 1963*b*) and subsequently there have been attempts to detect this experimentally (Lockett &

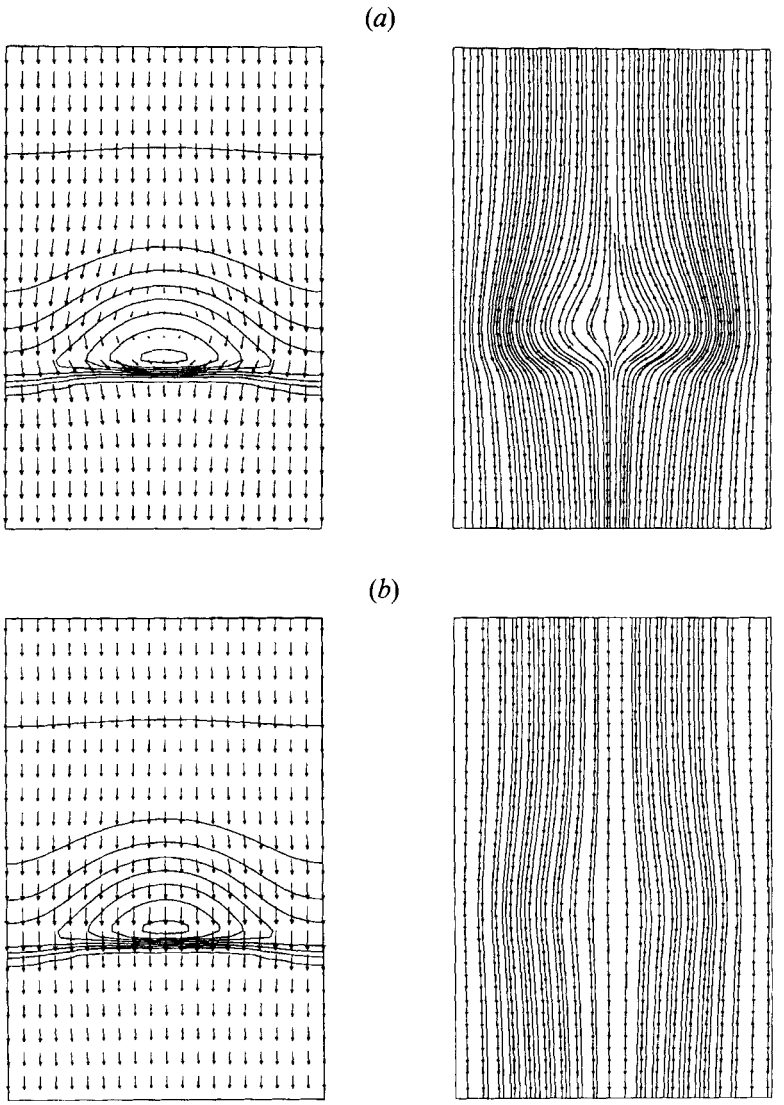

FIGURE 11. Velocity fields for the solution of figure 10 at $\tilde{t} = 0.36$: (*a*) fluid velocity (longest vector = $1.69u_0$); (*b*) solids velocity (longest vector = $3.48u_0$). $\tilde{v}_f = 0.936$ ($v_f = 2.27u_0$).

Harrison 1967; Nguyen, Leung & Weiland 1973), culminating in recent X-ray studies of Yates, Cheesman & Sergeev (1994), which seem to establish its existence beyond doubt. However, Yates *et al.* also found that the wake was a region of lower particle concentration, in contrast with the results in figure 10.

In the fluidization literature the observed velocity of rise of a bubble in a fluidized bed has often been compared with the velocity of the well-known Davies–Taylor bubble of the same diameter, d_b:

$$U_b = \frac{2}{3}\left[gd_b\left(1-\frac{\rho_v}{\rho_b}\right)\right]^{1/2},$$

where ρ_v denotes the density of the material within the bubble and ρ_b the density of the material outside. The precise 'diameter' of the bubble in figure 10(*d*) is a matter of

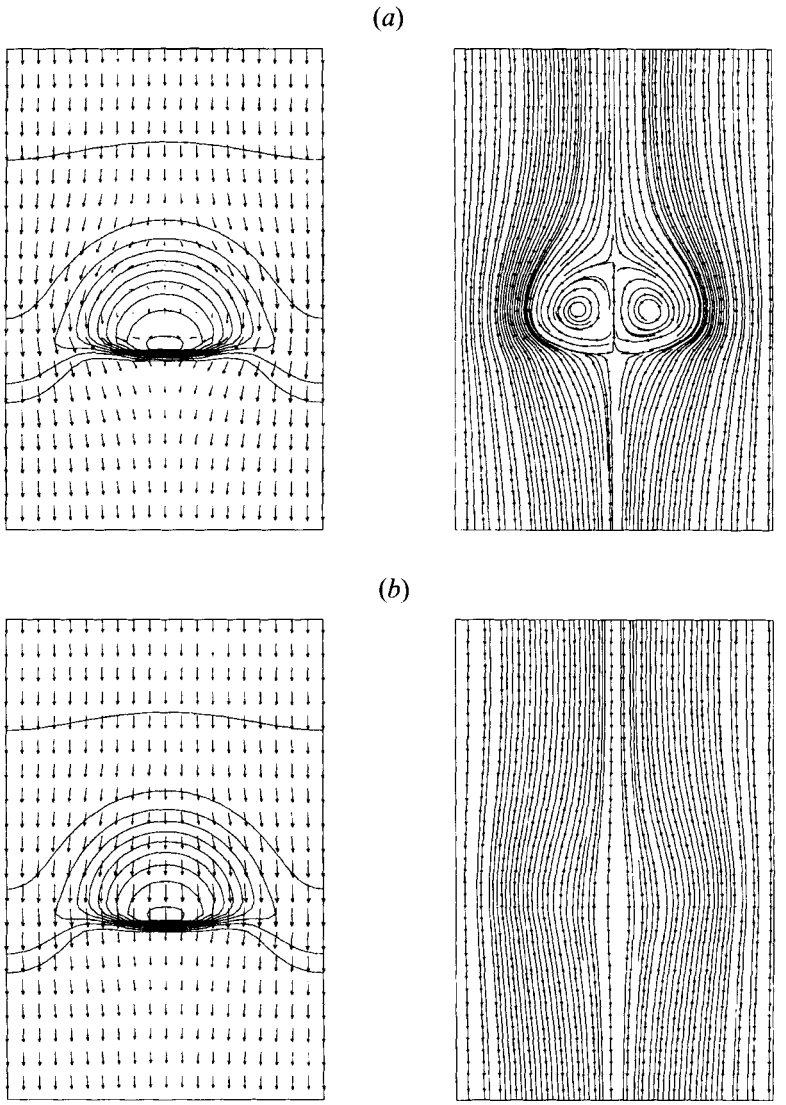

FIGURE 12. Velocity fields for the solution of figure 10 at $\tilde{t} = 0.58$: (*a*) fluid velocity (longest vector $= 2.35u_0$); (*b*) solids velocity (longest vector $= 3.92u_0$). $\tilde{v}_f = 1.03$ ($v_f = 2.48u_0$).

choice, since there is no sharply defined surface, but a value of the order of 2 cm is clearly reasonable. In the present case, where $\rho_v/\rho_b \approx 0.15/0.57$, for a bubble of diameter 2 cm the above formula gives $U_b = 25.3$ cm s^{-1} $= 2.77u_0$, very close to the value $2.76u_0$ found from the computations. Of course, this is largely fortuitous in view of the somewhat arbitrary choice of diameter. Furthermore the value of the Reynolds number for this bubble, based on the density of the undisturbed bed and viscosity $\mu_s^0 = 7.6$ g cm^{-1} s^{-1}, is only 8.35, not large enough to justify drawing an analogy with the Davies–Taylor bubble.

Since the rise velocity of the computed bubble is larger than the fluidization velocity the well-known and simple argument of Davidson (1961) indicates that the rising bubble should be accompanied by a 'cloud' of gas which moves with it, and within which there is a closed circulation. Figures 11–13 trace the development of this by

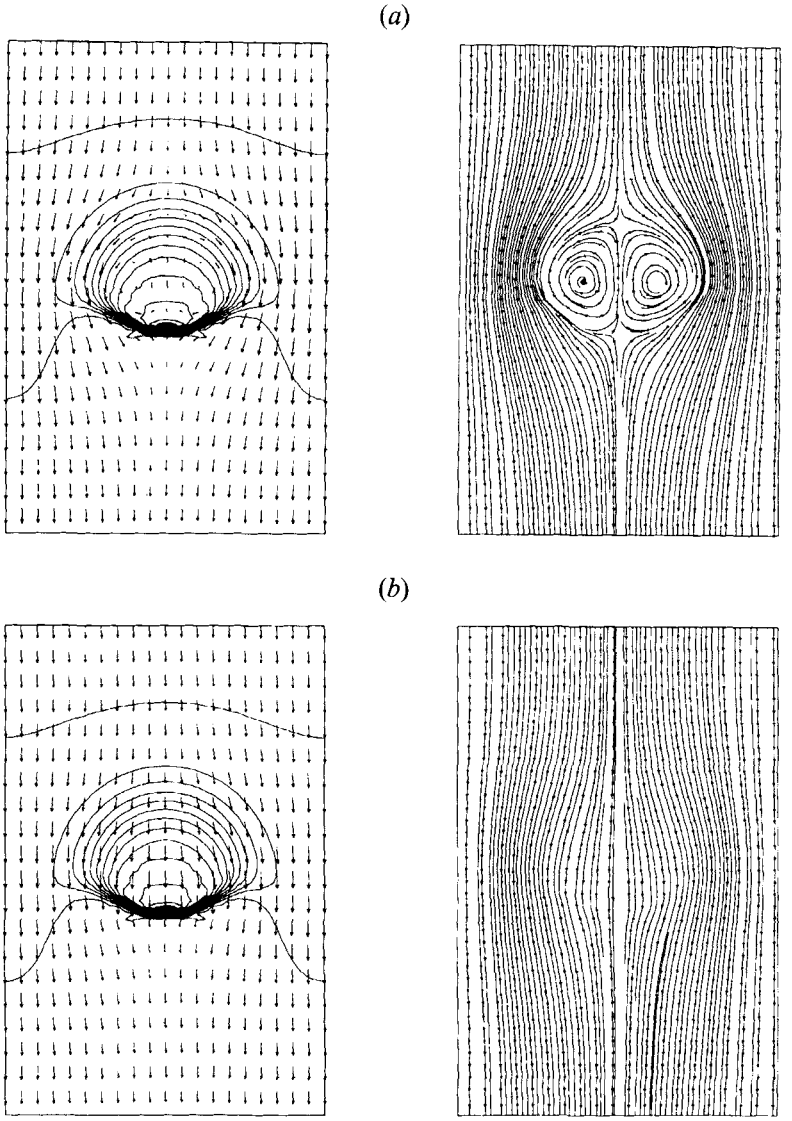

FIGURE 13. Velocity fields for the solution of figure 10 at $\tilde{t} = 0.75$: (*a*) fluid velocity (longest vector $= 2.84u_0$); (*b*) solids velocity (longest vector $= 4.52u_0$). $\tilde{v}_f = 1.14$ ($v_f = 2.76u_0$).

showing the fluid and particle velocity fields corresponding to the last three panels of figure 10, using the format already described for figure 8. (The velocity fields at $\tilde{t} = 0$, corresponding to the first panel, are not shown since they differ only slightly from those of the one-dimensional wave.) The closed circulation in the fluid flow has not yet appeared at $\tilde{t} = 0.36$, but it is well established by $\tilde{t} = 0.58$. At $\tilde{t} = 0.75$ note that the centre of the vortex lies somewhat above the region of lowest particle concentration, as was predicted by early attempts at a solution representing bubble motion (Jackson 1963*b*) and is observed experimentally. Note also that the closed streamlines extend out into regions of quite high particle concentration. The largest value of the upward fluid velocity (relative to the bubble) on the axis of the vortex is about one third of the rise velocity of the bubble in the rest frame. It has been speculated (Davidson & Harrison 1963) that these two velocities should be approximately equal and,

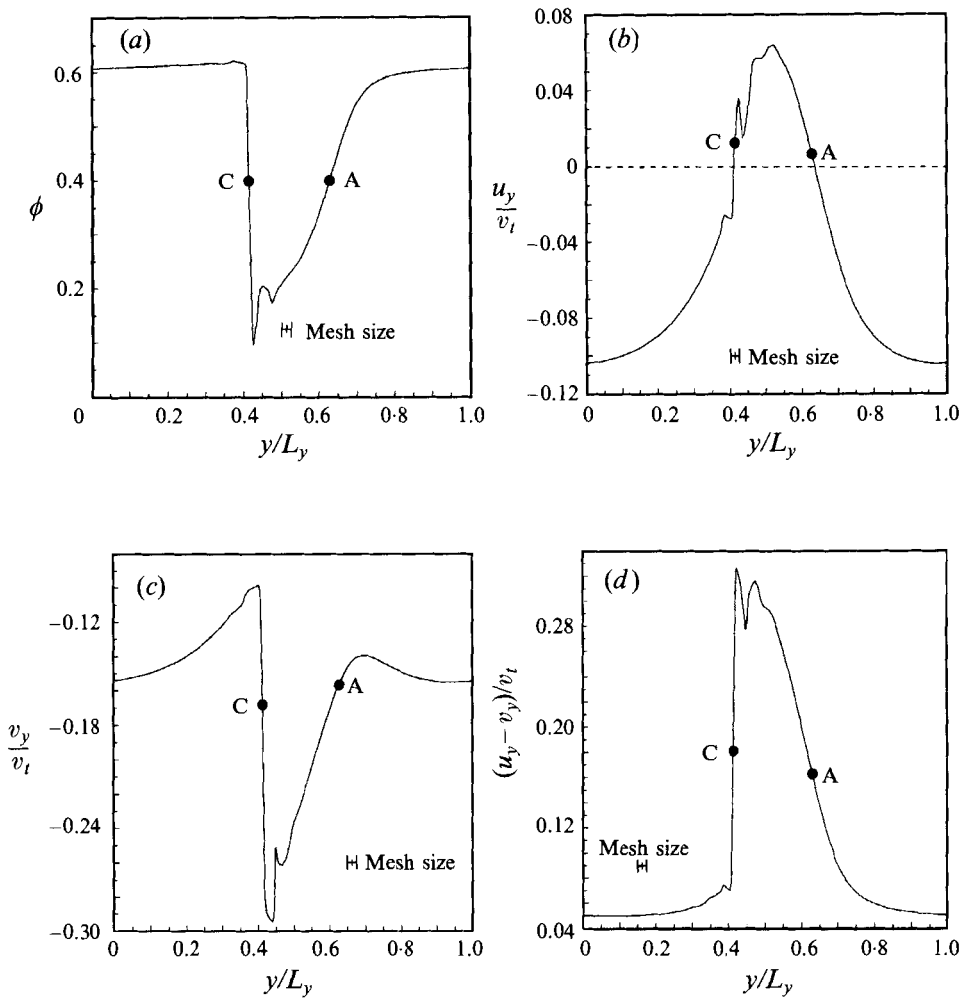

FIGURE 14. Quantities of interest plotted along the y-axis of the solution shown in figure 10(d): (a) solids volume fraction, (b) fluid velocity, (c) solids velocity, (d) slip velocity. For (b) and (c) $v_f = 2.75u_0$. Labels A and C identify corresponding points on each panel.

remembering that our numerically generated bubble is by no means free of particles and is still developing, our result verifies that they are, indeed, of the same order of magnitude.

It is instructive to examine in more detail the spatial variation of several important quantities along the vertical centreline of the cell; that is, the axis of symmetry of the bubble. Figure 14(a–d) shows the solids volume fraction and the fluid velocity, the solids velocity and the relative velocity as multiples of the terminal velocity v_t. Note the sharp spike, of width approximately equal to the size of the computational element, which appears at the minimum of the solids volume fraction and is reflected in all the other curves. This is to be expected, for the reason given above, and its presence warns that the bubble cannot be grown any further without resort to a finer subdivision of the cell into elements. The points labelled A and C in figure 14(a) identify the two positions where the solids volume fraction takes the value 0.4. They may arbitrarily be taken to indicate the roof and floor of the bubble, respectively, and the corresponding pairs of points are labelled in the same way in the other panels. Figure 14(b) reveals

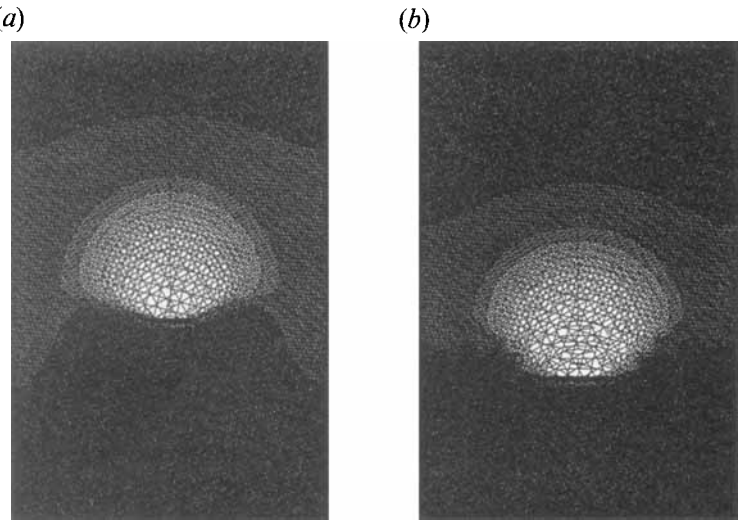

FIGURE 15. Density distribution at $\tilde{t} = 0.75$ for the bubble with $L_y = 3\lambda_m$, $L_x = 2\lambda_m$ in the air-fluidized bed. (*a*) 20×40 mesh, (*b*) 10×40 mesh.

a bounded interval of y in which upflow of fluid is generated by the vortex, while 14(*c*) shows the downward acceleration of the particles as they fall from the roof, the sudden deceleration when they hit the high-concentration region which extends below the floor of the bubble, and the subsequent, more gradual acceleration down into the bulk of the bed. Figure 14(*d*) confirms that the relative velocity of the two phases becomes large within the bubble, as would be expected from the low concentration of particles, reaching about one third of the terminal velocity of fall of an isolated particle. The largest value attained by u_y/v_t is approximately 0.065, so the upward circulation of gas does not become nearly strong enough to lift an isolated particle upward relative to the bubble.

The solution illustrated in figures 10–13 was generated with the rectangular cell shown divided into a grid of elements with twenty divisions in the horizontal direction and forty in the vertical direction. An idea of the adequacy of this subdivision can be obtained from figure 15, where figure 10(*d*) is reproduced, together with the corresponding density distribution computed using a grid of only 10×40 elements. The most noticeable difference is seen around the base of the bubble, where numerical artifacts on the scale of the elements appear in the solution generated using the coarser grid.

The above results appear to give a plausible representation of the growth of a regular two-dimensional array of bubbles in a fluidized bed, and establish that relatively simple equations of motion contain the physics needed to account for their salient observed features. The predicted bubble shape is not quite like shapes observed in 'two-dimensional' fluidized beds; for example, we do not see the typical form of the floor of the bubble. However, a limited number of calculations with a viscosity μ_s independent of solids volume fraction, in contrast to the expression (10) used in the present computations, has indicated that the detailed shape of the bubble floor can be modified quite significantly by a change in the rheology of the particle assembly (B. Glasser 1994, personal communication).

The route by which we arrived at the bubble shown in figure 10(*d*) is rather special, since we chose first to constrain the perturbation of the uniform bed to be one-

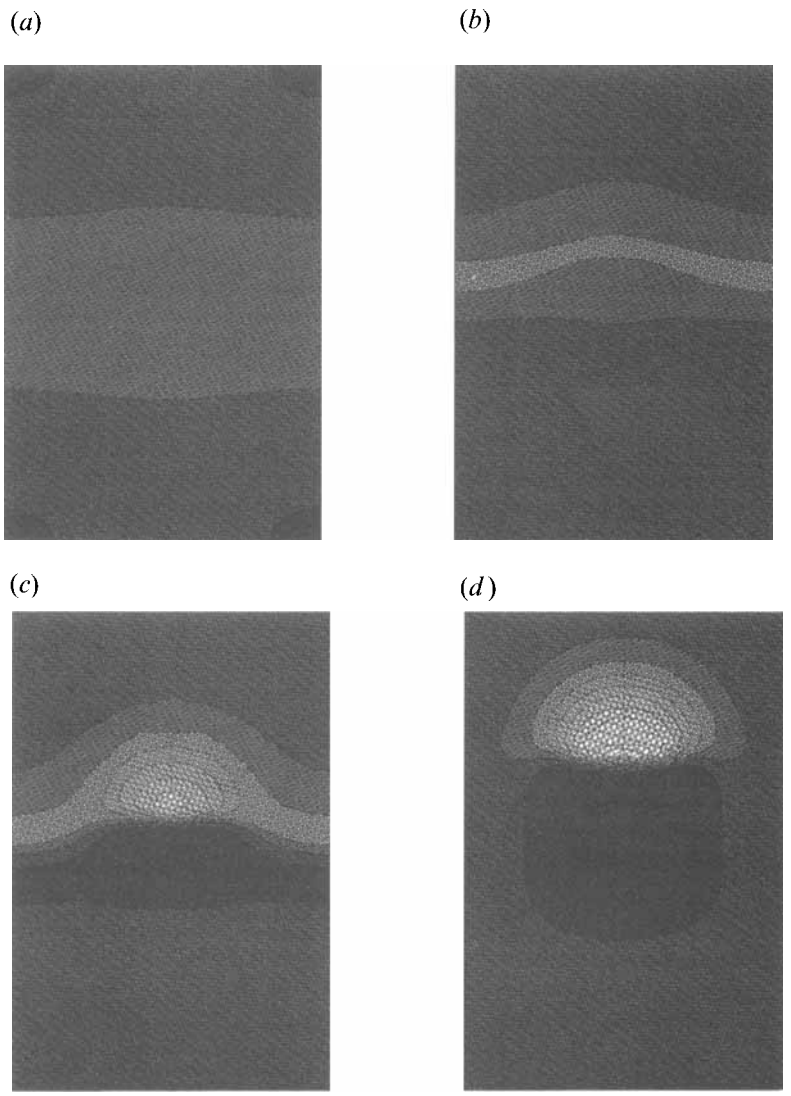

FIGURE 16. Growth of a small, initially two-dimensional perturbation of the uniform air-fluidized bed ($\phi' = 0.02, \epsilon = 0.1$), $L_y = 3\lambda_m$, $L_x = 2\lambda_m$. 20×40 element mesh. $\Delta t^* = 0.01$. (*a*) $\tilde{t} = 0$, (*b*) $\tilde{t} = 0.44$, (*c*) $\tilde{t} = 0.91$, (*d*) $\tilde{t} = 1.35$.

dimensional, only relaxing this restriction when the one-dimensional growth was essentially complete. By this route the elapsed times for the computed growth of the one-dimensional wave, and for the subsequent development of the two-dimensional structure, are similar. The question then remains whether the same type of bubble will grow from a small perturbation of the uniform bed which has a two-dimensional structure from the start. To answer this a perturbation was constructed by specifying a spatial distribution of solids volume fraction with the form

$$\phi(x, y, 0) = \phi_0 + \phi' \cos(2\pi y/L_y)[(1-\epsilon) + \epsilon \cos(2\pi x/L_x)], \tag{15}$$

then deducing the corresponding velocity perturbations from the explicitly known solutions of the linearized equations. In (15) ϕ' measures the overall amplitude of the initial perturbation, while ϵ is a measure of its two-dimensional nature.

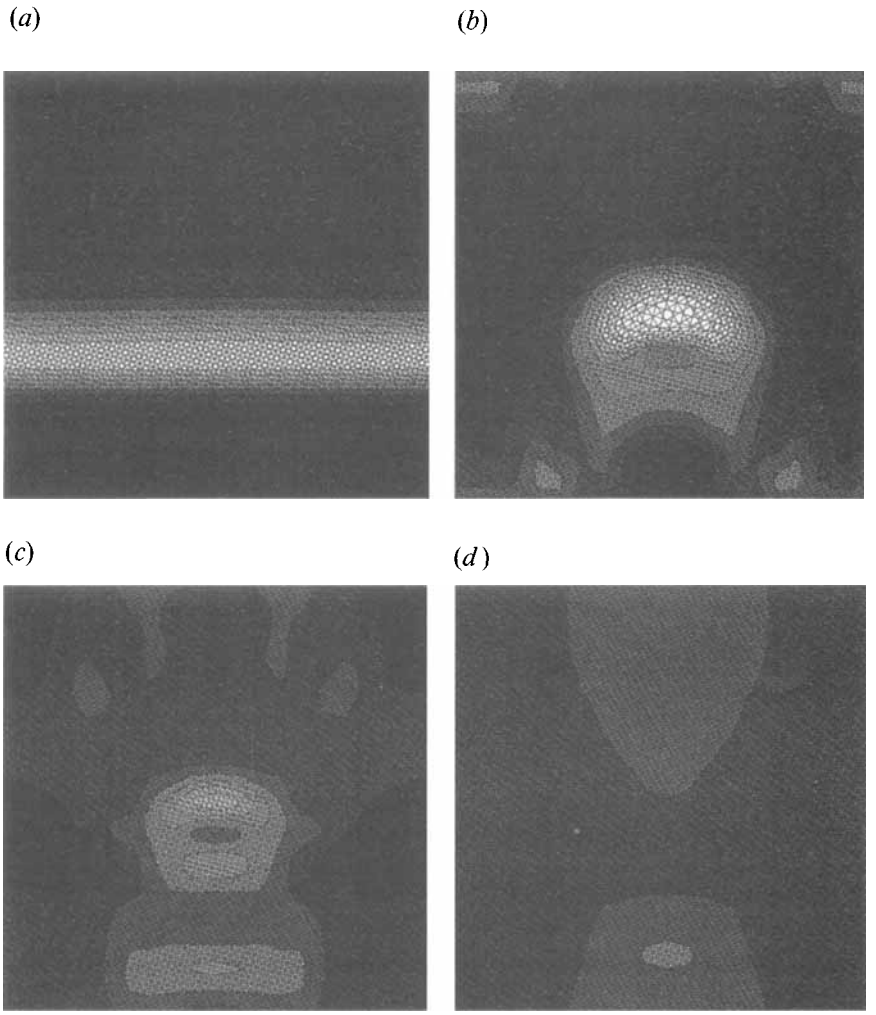

FIGURE 17. Two-dimensional growth of the perturbed fully-developed one-dimensional wave of wavelength $3\lambda_m$ in the water-fluidized bed. $L_y = 3\lambda_m$, $L_x = 3\lambda_m$. 10×40 element mesh. $\Delta t^* = 0.01$. (*a*) $\tilde{t} = 0$, (*b*) $\tilde{t} = 0.033$, (*c*) $\tilde{t} = 0.075$, (*d*) $\tilde{t} = 0.18$.

Numerical solutions of the full nonlinear equations were generated from initial conditions of the type (15), with $\phi' = 0.02$ and three different values of ϵ, namely 0.001, 0.01 and 0.1. In each case the initial development is found to be dominated by the one-dimensional component of the disturbance, which grows fastest. As the amplitude of the one-dimensional structure increases, the presence of the small lateral non-uniformities activates the lateral instability mechanism and, as a result, the bubble-like solution is eventually reached in all three cases. This is illustrated by figure 16, which shows the solids volume fraction at a sequence of increasing values of the time for the case $\epsilon = 0.1$. After an initial period during which the disturbance changes shape, but does not deepen very much, growth becomes rapid, and at $\tilde{t} = 1.35$ a perfectly recognizable bubble has developed. This corresponds closely to the structure depicted in figure 10(*c*), so further development is expected to be similar in both cases. Thus, we have established that essentially the same bubble-like solution develops by quite different routes, and is not peculiar to the constrained path depicted in figure 10.

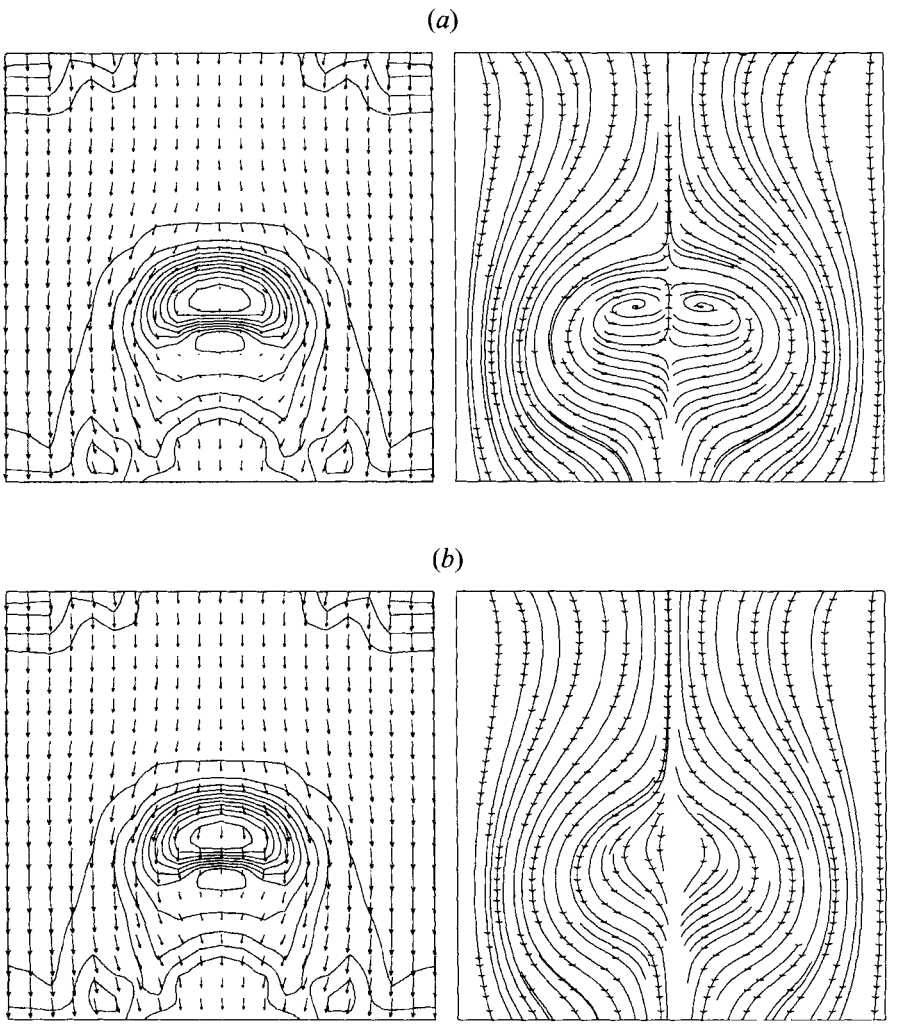

FIGURE 18. Velocity fields for the solution of figure 17 at $\tilde{t} = 0.033$: (*a*) fluid velocity (longest vector = $7.17u_0$), (*b*) solids velocity (longest vector = $7.86u_0$). $\tilde{v}_f = 2.68$ ($v_f = 5.58u_0$).

7. Two-dimensional motions in the water-fludized bed

The results presented above indicate that equations of motion of the type proposed can account for spontaneous bubble formation in a typical gas-fluidized bed. It remains to be seen whether the same equations will also predict an absence of bubbles from the liquid-fluidized bed. To treat the liquid case only the following parameter values are altered.

(i) The density and viscosity, ρ_f and μ_f, are changed from those of air to those of water.

(ii) The parameters v_t and n in the Richardson–Zaki equation (17) are changed to the values appropriate for a suspension of 1 mm glass beads in water.

(iii) The parameter P in equation (9) is reduced so that the limiting solids volume fraction for stability retains the value 0.578, as for the gas-fluidized bed.

These changes are reflected in table 1.

The procedure is then the same as for the gas-fluidized bed, starting with an investigation of the growth of two-dimensional structures from a fully developed one-

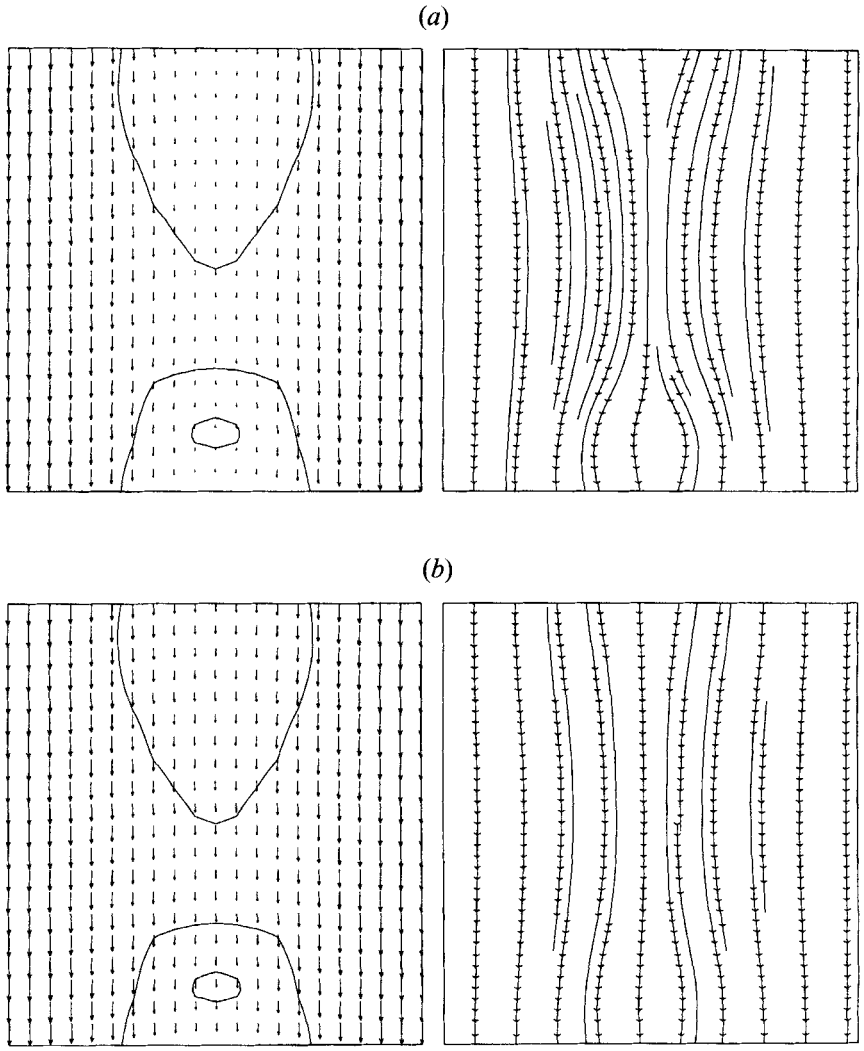

FIGURE 19. Velocity fields for the solution of figure 17 at $\tilde{t} = 0.18$: (*a*) fluid velocity (longest vector = $4.14u_0$), (*b*) solids velocity (longest vector = $5.0u_0$). $\tilde{v}_f = 1.70$ ($v_f = 3.54u_0$).

dimensional wave, namely that shown in figure 5(*c*). This is similar to the wave of figure 4(*c*) from which the corresponding calculation started for the gas-fluidized bed. Then $L_y = 3\lambda^m$, and the wave is stable when it is constrained to remain one-dimensional with this wavelength. Its stability to development in the second dimension is tested, as for the gas-fluidized bed, by increasing the width of the cell in the x-direction and observing the eigenvalues of the computational algorithm for two-dimensional perturbations of the one-dimensional travelling wave solution. These migrate in just the same way as described above for the case of the gas-fluidized bed. A real and positive eigenalue appears as the width is increased, reaching its largest value between $L_x = L_y$ and $L_x = 1.5L_y$. We did not attempt to locate, with any greater accuracy, the value of L_x which maximizes this eigenvalue, but studied the growth of disturbances in the square cell with $L_x = L_y = 3\lambda^m$. A small increment of the eigenfunction corresponding to this eigenvalue was added to the fully developed one-dimensional wave and the numerical integration was started from this initial condition.

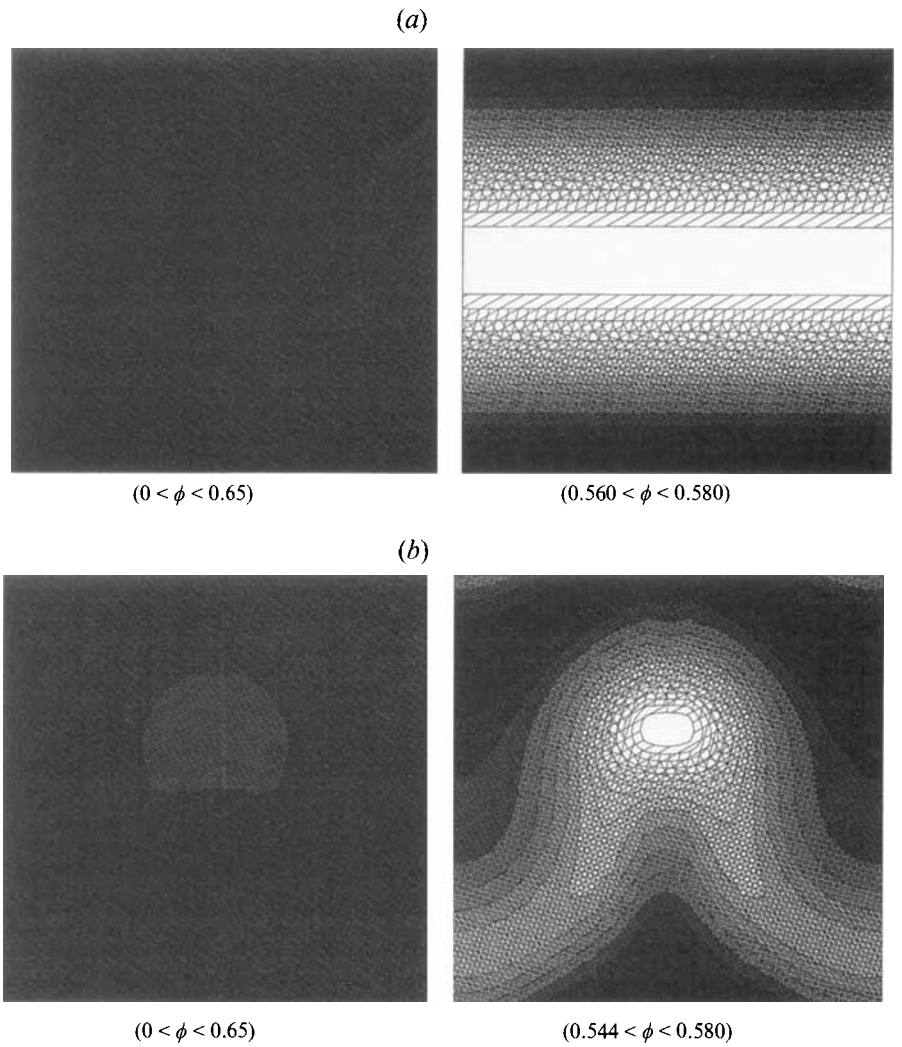

FIGURE 20 (*a*,*b*). For caption see facing page.

The computed solids volume fraction, at successively increasing values of the time, is shown in figure 17, while the fluid and particle velocity fields corresponding to figures 17(*b*) and 17(*d*) can be found in figures 18 and 19. Up to $\tilde{t} = 0.033$ (figure 17*b*) the development of the disturbance has some resemblance to what was seen for the air-fluidized bed. The wave bends upward on the centreline of the cell, a localized region of lower particle concentration develops at the apex of this bend, a fluid circulation develops in the same vicinity, and the particle streamlines bulge around this region. The minimum value of the solids volume fraction is about 0.15, so this concentration pattern comes as close to an empty bubble as anything found in the air-fluidized case (figure 10*d*). However, the dimensionless time $\tilde{t}$ required to reach this stage is less than one twentieth of the corresponding dimensionless time for the air-fluidized bed. In other words, the growth of the secondary two-dimensional instability, relative to that of the primary one-dimensional instability, is much faster in the liquid-fluidized bed. There are also other differences between the two cases. First, the shapes of the regions

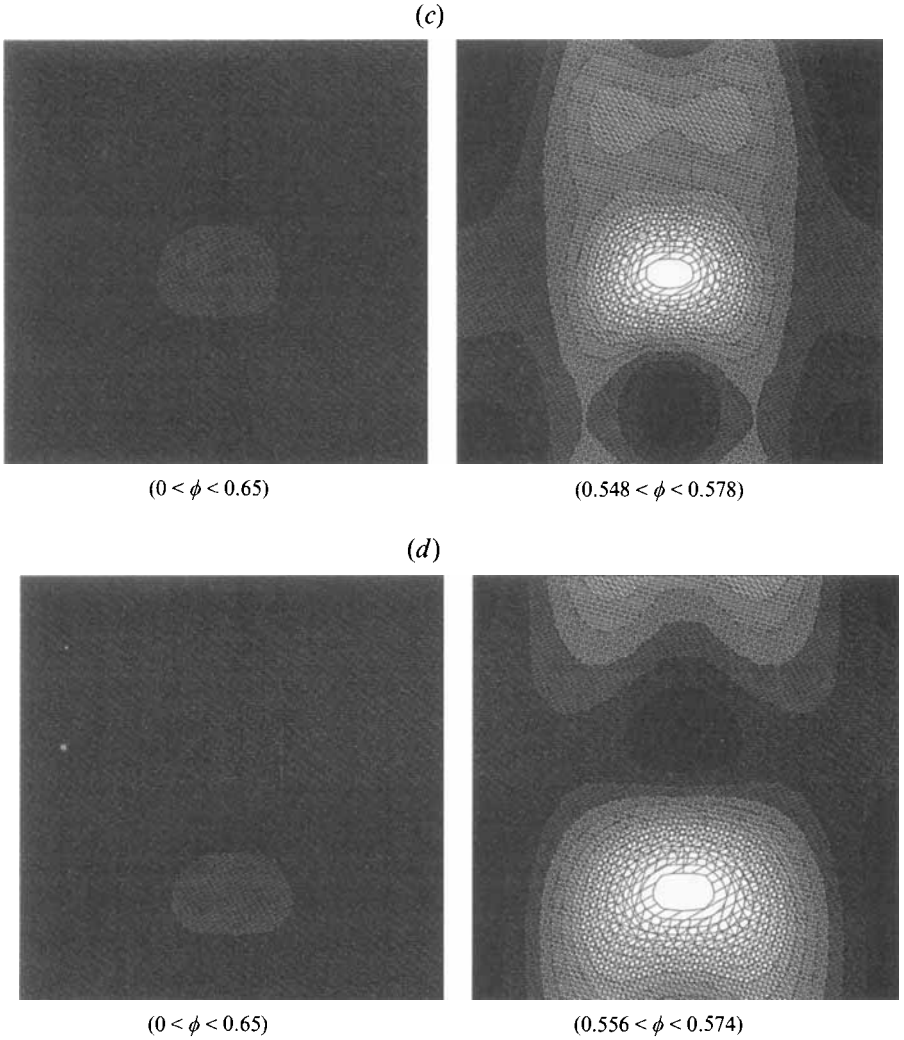

FIGURE 20. Growth of a small, initially two-dimensional perturbation of the uniform water-fluidized bed ($\phi' = 0.02, \epsilon = 0.001$), $L_y = 3\lambda_m$, $L_x = 3\lambda_m$. 10×40 element mesh. $\Delta t^* = 0.01$. (*a*) $\tilde{t} = 0$, (*b*) $\tilde{t} = 0.42$, (*c*) $\tilde{t} = 0.64$, (*d*) $\tilde{t} = 0.91$.

of low concentration are quite different, with material of higher particle concentration bulging up from below into the incipient bubble in the case of the water-fluidized bed. Second, the increase in speed of rise of the incipient bubble, relative to that of the one-dimensional wave, is much larger in the water-fluidized bed, where the starting wave speed is $2.05u_0$, while at $\tilde{t} = 0.033$ the region of low concentration has accelerated to a speed of $5.58u_0$. In contrast, for the air-fluidized bed, the speed changes only from $2.16u_0$ to $2.76u_0$.

When the integration is continued beyond this time the region of high concentration below the incipient bubble moves further up, eventually causing the bubble to fill in and become an insignificant feature, as seen in figure 17(*c*, *d*). By $\tilde{t} = 0.075$ the circulating vortex, associated with the region of low particle concentration, has become weak, and at $\tilde{t} = 0.18$ figure 19 shows that it has disappeared altogether. Note also that the speed of rise of the concentration pattern, relative to the rest frame, decreases again

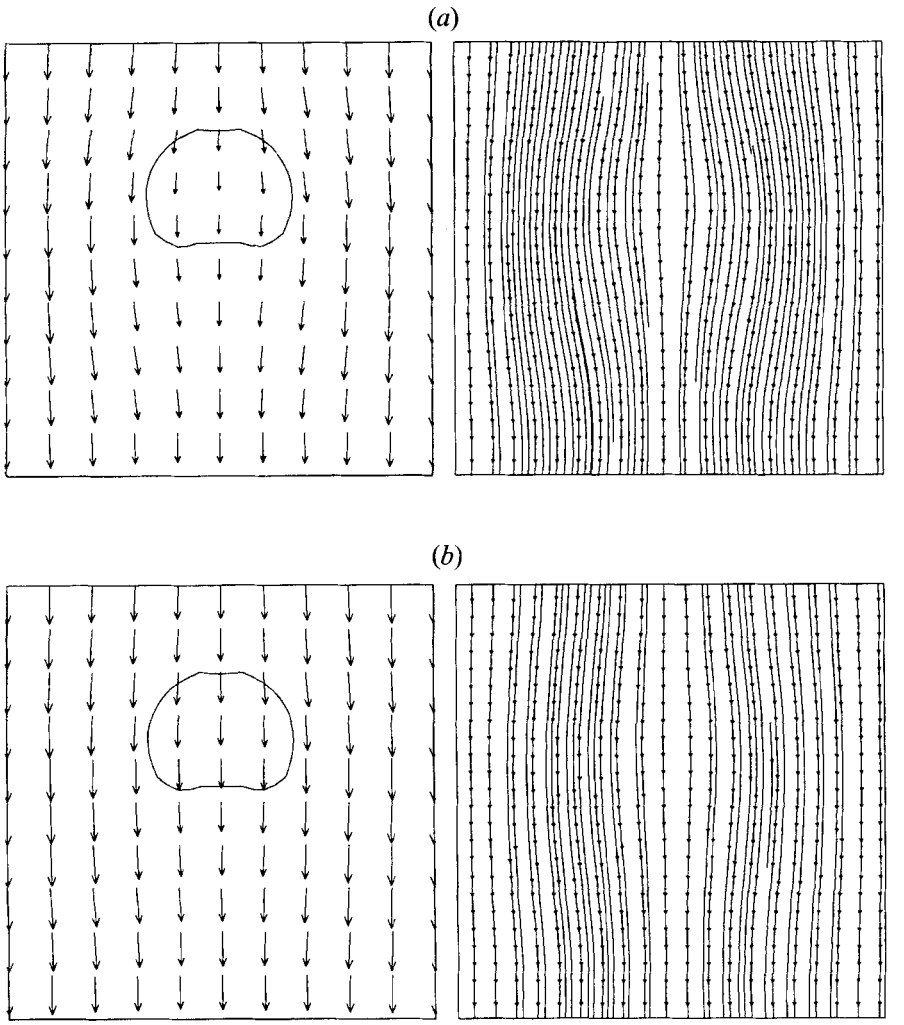

FIGURE 21. Velocity fields for the solution of figure 20 at $\tilde{t} = 0.42$: (*a*) fluid velocity (longest vector = $1.94u_0$), (*b*) solids velocity (longest vector = $2.87u_0$). $\tilde{v}_f = 1.17$ ($v_f = 2.44u_0$).

after $\tilde{t} = 0.033$, and has fallen to $3.54u_0$ at $\tilde{t} = 0.18$. The ultimate fate of the disturbance is uncertain, though it cannot decay completely since the uniformly fluidized state is unstable. Nevertheless, it is clear that the incipient bubble has only a brief transient existence in this case.

The mechanism by which the bubble is disrupted is reminiscent of an early suggestion of Davidson & Harrison (1963), who proposed that a bubble in a liquid-fluidized bed would be destroyed by particles moving up into it from the dense wake region below. In our solution the bubble is, indeed, destroyed by an intrusion of dense bed from below, but the vertical component of the particle velocity is directed downward everywhere, at all times. The rising heap of dense material is formed because particles rain down from the roof of the incipient bubble more rapidly than they can escape through the wake. This is the opposite of the situation in the gas-fluidized bed, where it is found that the rate of escape exceeds the flux descending from the roof as the bubble develops.

Instead of starting from a fully developed one-dimensional wave the integration can alternatively be started from a small two-dimensional perturbation (15) of the uniform fluidized bed, and the resulting distributions of solids volume fraction are shown in figure 20 for a very small initial degree of two-dimensionality ($\epsilon = 0.001$). The left-hand panel of each pair shows the solids volume fraction on an absolute scale (white represents $\phi = 0$ and black $\phi = \phi_p = 0.65$), while the right-hand panel uses an expanded scale to reveal details of the very small concentration variations. It is seen that there is little growth of the initial density perturbation. On the absolute scale a compact region of slightly reduced solids volume fraction can be discerned, and the expanded scale shows that its development is at first qualitatively similar to that of the corresponding, but much more vigorous, phenomenon in the air-fluidized bed, shown in figure 16. However, when $\tilde{t} > 0.42$, the minimum particle concentration begins to increase again, so the shallow 'hole' begins to fill in. Figure 21 shows the velocity fields at the time the concentration perturbation is largest, namely $\tilde{t} = 0.42$, and it is seen that no vortex has formed in the fluid flow; indeed, the streamlines of both phases are scarcely bent away from the vertical. Thus, in contrast to the case of the air-fluidized bed, a slightly two-dimensional perturbation of the uniform water-fluidized bed fails to grow to any significant extent. This appears to be a consequence of the much larger ratio of the time scales for one- and two-dimensional growth in the water-fluidized bed. In the water-fluidized case the uniform bed has no unstable eigenvalues belonging to two-dimensional eigenfunctions, and the small degree of two-dimensionality in the applied perturbation actually begins to decay initially. However, as soon as the growth of the unstable one-dimensional mode generates layers of alternating higher and lower bulk density, the two-dimensional instability rapidly asserts itself and overwhelms the relatively slow growing one-dimensional wave.

The concentration distributions attained in the water-fluidized bed after some time can be quite complicated but, when tested by integrating with a different size of spatial elements, and with different time steps, they proved to be reproducible. The same patterns are also seen in solutions obtained by a completely different numerical method (B. Glasser 1994, personal communication).

8. Discussion

We begin by examining the time scale for the growth of two-dimensional perturbations of the fully developed one-dimensional waves. The one-dimensional waves are asymmetric and do not have a simple algebraic representation in closed form, so explicit expressions for the growth parameters of small perturbations cannot be found by linearization. However, Batchelor & Nitsche (1991) have analysed the stability of a fluid whose density is sinusoidally modulated in the vertical direction:

$$\rho = \rho_0(1 + A\sin(\kappa y)) \tag{16}$$

subject to perturbations of the form $\exp(\gamma t)\cos(\alpha x)$. The density variation was assumed to be the result of variations in concentration of some suspended or dissolved material (the particles in the situation of interest here) and equations describing the evolution of the disturbance were formulated in terms of an average velocity, with a term to represent diffusion of this material. Thus the continuity equation was written in the form

$$\frac{\partial \phi}{\partial t} + \boldsymbol{u}_v \cdot \boldsymbol{\nabla}\phi = D\nabla^2\phi = \boldsymbol{\nabla} \cdot (D\boldsymbol{\nabla}\phi), \tag{17}$$

where D is a diffusion coefficient and $\boldsymbol{u}_v$ denotes the mixture velocity, i.e. $\phi\boldsymbol{v}+(1-\phi)\boldsymbol{u}$ in our case. (The two forms for the right-hand side of (17) are equivalent if D is assumed constant, as in Batchelor & Nitsche, but the second form is the correct one if D depends on ϕ.) The mixture was also assumed to be viscous, with a kinematic viscosity denoted by ν. Then introducing the following dimensionless groups:

$$s=\frac{\gamma}{(\kappa g A)^{1/2}};\quad x=\frac{\alpha}{\kappa};\quad R'=\frac{gA}{\nu^2\kappa^3};\quad \frac{\nu}{D}$$

Batchelor & Nitsche's equation for the growth rate of the dominant perturbation ((5.17) of their paper) can be written as

$$(sR'^{1/2}+x^2)(sR'^{1/2}+x^2+1)\left(s\frac{\nu}{D}R'^{1/2}+x^2\right)\left(s\frac{\nu}{D}R'^{1/2}+x^2+1\right)=\frac{1}{2}\left(\frac{\nu}{D}\right)^2\frac{R'^2x^2}{1+x^2}. \quad (18)$$

The dimensionless growth rate s_m for the fastest growing two-dimensional perturbation is then found by finding the largest root of (18) and maximizing it with respect to x.

The parameter values quoted in tables 1 and 2 permit R' to be calculated for stratified fluids corresponding to the fully developed one-dimensional wave structures in the gas- and liquid-fluidized beds treated in this paper. Appropriate values for the diffusion coefficient D can also be identified using the following argument. A description of the relative motion of particles and fluid by a dispersion term, as in (17) above, is appropriate when that motion results only from a gradient in concentration, and inertial effects associated with it are negligible. Then, in terms of the equations of the present paper

$$0=-\nabla p_s+\beta(\phi)(\boldsymbol{u}-\boldsymbol{v})$$

or, if $\boldsymbol{w}=\boldsymbol{v}-\boldsymbol{u}$,

$$\boldsymbol{w}=-\frac{\nabla p_s}{\beta}=-\frac{p_s'}{\beta}\nabla\phi. \quad (19)$$

The fluid and particle phase velocities can then alternatively be expressed in terms of $\boldsymbol{w}$ and $\boldsymbol{u}_v$; in particular $\boldsymbol{v}=\boldsymbol{u}_v+(1-\phi)\boldsymbol{w}$. The sum of the particle and fluid continuity equations, (1) and (2), then shows that $\nabla\cdot\boldsymbol{u}_v=0$, and the continuity equation for the particles can be written in terms of $\boldsymbol{u}_v$ and $\boldsymbol{w}$ as

$$\frac{\partial\phi}{\partial t}+\boldsymbol{u}_v\cdot\nabla\phi=-\nabla\cdot[\phi(1-\phi)\boldsymbol{w}]$$

or, using (19),

$$\frac{\partial\phi}{\partial t}+\boldsymbol{u}_v\cdot\nabla\phi=\nabla\cdot\left[\frac{\phi(1-\phi)p_s'}{\beta}\nabla\phi\right]. \quad (20)$$

This has the same form as (17), so the diffusion coefficient can be related to p_s' and β:

$$D(\phi)=\frac{\phi(1-\phi)p_s'(\phi)}{\beta(\phi)}. \quad (21)$$

Finally, from (16) $A=\Delta\rho/\rho_0$, where $\Delta\rho$ is the difference between the highest and lowest densities of the stratified fluid, and in applying the above analysis to our fully developed pattern of one-dimensional waves this can be determined from figures 4(*c*) and 5(*c*), for the gas- and liquid-fluidized beds, respectively. Thus, values of s_m and x_m can be calculated from (18) then compared with the same quantities found from the dominant eigenvalue of our computational algorithm for small two-dimensional

	R'	ν/D	s_m (B&N)	x_m (B&N)	s_m (ASJ)	x_m (ASJ)
Air-fluidized bed; $\tilde{L}_y = 3$	35.05	5.5	0.567 (9.04 s^{-1})	0.97	0.387 (6.18 s^{-1})	≈ 1.5
Water-fluidized bed; $\tilde{L}_y = 3$	7.10	542	0.491 (7.44 s^{-1})	0.88	0.244 (3.70 s^{-1})	≈ 1.0

TABLE 4. Properties of a two-dimensional perturbation of the fully developed one-dimensional waves. B & N denotes values calculated by the method of Batchelor & Nitsche; ASJ denotes results from the computational algorithm of the present paper. $\tilde{L}_y$ denotes the wavelength of the fully developed one-dimensional wave, expressed as a multiple of the wavelength of the fastest growing small perturbation of the uniform bed (see figures 4*c* and 5*c*). In the last column it is indicated that the values of x_m were determined only approximately in the present work, since the maximum of s_m was quite flat.

perturbations of the fully developed one-dimensional waves. Such a comparison is presented in table 4, from which it is seen that the growth rates calculated by the method of Batchelor & Nitsche are between one and a half and two times those computed in the present work. The wavelengths of the lateral perturbations which grow most rapidly, found from Batchelor & Nitsche, are somewhat longer than those determined in the present work, though no attempt was made to identify these with great precision. Note that the dimensional growth rates (given in brackets below their dimensionless counterparts) are of the same order of magnitude for the air- and water-fluidized beds, whether they are found as in Batchelor & Nitsche or from our computational algorithm.

Exact agreement between our results and those of Batchelor & Nitsche should not be expected since sedimentation of the particles is not accounted for in their work (though it is included in a later paper (Batchelor 1993)), and the horizontal striations, which form the base states in our work, are not sinusoidal like theirs. Since we have computed solutions for only two isolated cases, not too much should be read into the figures quoted in table 4. However, they provide some support for the view that the Batchelor–Nitsche stability analysis provides a reasonable and easily calculated estimate of the time scale for the secondary instability.

Dimensional analysis applied to the problem of Batchelor & Nitsche shows directly that there exists a functional relation of the form

$$s_m = f(R', \nu/D) \tag{22}$$

and solution of (18) permits this relation to be computed. If the dependence of f on R' and ν/D were weak, then it would follow that the growth rate, γ, would scale like $(\kappa g \Delta\rho/\rho_0)^{1/2}$, as recently speculated by E. J. Hinch (1994, personal communication). However, s_m is found to be quite strongly dependent on R', so this simple scaling is not adequate.

The secular equation for the problem of linear stability of the uniform fluidized bed can also be cast in dimensionless form, in various ways. For example, it can be shown that there exists a dimensionless functional relation of the form

$$s_m = f\left(\frac{c_u}{V}, \frac{c_d}{V}, \frac{v_v}{V}\right) \tag{23}$$

where, as before, V, c_u and c_d are the velocities of the continuity wave and the upward and downward dynamic waves, v_v is a velocity which depends on the kinematic

viscosity of the uniform bed, and s_m is the growth rate of the fastest growing perturbation, in dimensionless form. s_m and v_v are defined as follows:

$$s_m = \frac{\nu\sigma_{rm}}{CV^2}; \quad v_v = \frac{1}{C}\left[\frac{\nu g}{u_0}\left(\frac{(\rho_s-\rho_f)/\rho_s}{1-\phi_0}\right)\right]^{1/2},$$

where σ_{rm} is the dimensional growth rate for the fastest growing mode and C is a dimensionless factor given by

$$C = 1+\frac{\rho_f}{\rho_s}\frac{\phi_0}{1-\phi_0}.$$

The relation (23) can easily be computed, since the secular equation is merely a quadratic in this case, but s_m is found to depend quite strongly on c_u/V and c_d/V, so no simple scale factor for the growth rate emerges. In this respect alternative methods of rendering the secular equation dimensionless appear to fare no better.

We must conclude that simple explicit scalings for the growth rates of the primary, one-dimensional disturbance and the secondary two-dimensional instability of the equilibrated one-dimensional waves probably cannot be found. Nevertheless, the former can easily be estimated from the linear stability analysis of the uniform bed and there is an indication that the latter may be approximated from the Batchelor–Nitsche theory of stability of a striated fluid. The ratio of these time scales is important as it seems to play a significant role in determining whether or not bubbles appear in the bed.

A second factor which seems to be important is the degree of asymmetry of the fully developed one-dimensional waves. As noted earlier, comparison of figures 4(*c*) and 5(*c*) reveals that the density profile for a fully developed wave in the air-fluidized bed is markedly asymmetric. The layer of low particle concentration is bounded below by a sharp interface, across which the solids volume fraction rises suddenly to about 0.61. In contrast, the upper boundary is diffuse, with the concentration rising to about 0.61 over a distance of the same order as the width of the low-concentration layer itself. For the water-fluidized bed the asymmetry, though still present, is much less marked. This difference between the one-dimensional waves in the two beds is reflected in the eigenfunctions representing the fastest growing two-dimensional perturbations of these waves. Figure 10(*a*), which superposes the one-dimensional wave and a perturbation proportional to this eigenfunction, reveals a marked 'buckling' of the upper more diffuse boundary of the low-concentration layer, but very little buckling of the sharper lower boundary. In the initial stages of the subsequent motion it is seen from figure 10(*b*) that the buckling of the upper boundary continues, while the lower boundary distorts very little. The effect of this is to generate a region of increasing size, within which the particle concentration is further reduced, and it is this region which then continues to grow into the bubble. Only in the later stages of growth (figure 10*c*, *d*) does the lower boundary of the layer of low concentration buckle and, even then, marked buckling is confined to those parts outside the bubble.

For the water-fluidized bed figure 17(*a*) replaces figure 10(*a*), and here there is nothing like the same contrast between the appearance of the upper and lower boundaries of the layer of low concentration. As time passes both buckle at a comparable rate, with the upward bulge of the upper boundary matched by a similar upward bulge of the lower boundary. This can be seen in figure 17(*b*), which should be compared with figure 10(*b*, *c*). Though a small pocket of quite low concentration forms in the apex of this bulge (figure 17*b*), it is subsequently eliminated as the buckling

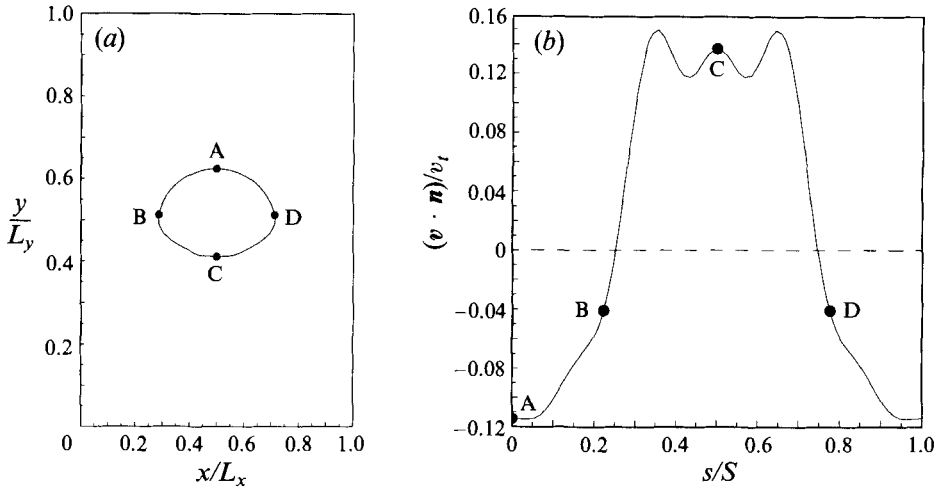

FIGURE 22. (*a*) Contour $\phi = 0.4$ from solids fraction distribution of figure 10(*d*). (*b*) Outward normal component of flux velocity of particles through curve shown in (*a*).

of the lower boundary causes the region of high density below to move up into it. As mentioned earlier, this is strongly reminiscent of a mechanism proposed by Davidson & Harrison (1963), though in our case the motion of the particles is everywhere downward in the rest frame of the incipient bubble; the region of high density ascends into the bubble because particles fall onto its upper surface faster than they can escape below.

When a bubble in the air-fluidized bed is already well formed, as in figure 10(*d*), it is interesting to trace which features of the particle flow field are responsible for its continued emptying. To see this consider figure 22, which corresponds to a growing bubble in the air-fluidized bed at the stage represented by figure 10(*d*). The closed curve in figure 22(*a*) is the contour $\phi = 0.4$ from figure 10(*d*), which we may arbitrarily choose to regard as the boundary of the bubble, and figure 22(*b*) then plots the outward normal component of the solids velocity (and hence the flux of solid material) as a function of position around this contour. Four corresponding pairs of points are labelled with the same letters to help in relating the two diagrams. It is seen that the solids flux out of the boundary at the floor (point C) is slightly larger than the flux in at the roof (point A). This difference, which is entirely responsible for growth in the case of the one-dimensional waves, has become quite small at this stage of development of the two-dimensional structure. More significant is the efflux of particles at points about midway between B and C, and between D and C, which is not balanced by the much smaller influx at points midway between B and A, and between D and A. Comparing this figure with figure 10(*d*), it is seen that these unbalanced outflows are located roughly where a dense region behind the bubble gives way to a band of smaller density, which is the (much distorted and attenuated) remnant of the original one-dimensional layer out of which the bubble grew. The lower surface of this layer is inclined steeply, and the effluxes near the points where it meets the bubble may simply reflect the fact that sedimentation of the particles through this layer offers an alternative to escape from the bubble by sedimentation through the denser wake directly below it.

Recently Batchelor & Nitsche (1994) have explored the final stages of expulsion of particles from a bubble by computing trajectories of individual particles in interaction

with the circulating gas within the bubble. For particles of diameter 60 μm and smaller they found that the particles deviated from the gas streamlines as a result of centrifugal force, causing them to spiral outward and eventually leave the bubble. For 80 μm particles (and presumably larger particles also), on the other hand, they found that particles exited the bubble by falling through its floor, so that is what we would expect in the case treated here. However, this cannot be verified from our computations, since these terminate when the bubble still contains more than 15% solids by volume.

For perturbations of the uniform bed which start with some two-dimensional structure the vital difference between the air- and water-fluidized beds lies in the relative time scales of the primary and secondary instabilities. In the air-fluidized case these are both of the same order of magnitude, so the primary instability has an opportunity to develop to a point where it has generated bands with significant contrast in particle concentration before it is overcome by the secondary instability. In the water-fluidized case, on the other hand, the time scale of the secondary instability is an order of magnitude faster than that of the primary instability. Consequently the secondary instability develops before the primary instability has had an opportunity to generate any significant contrast in particle concentration between adjacent bands. The primary instability is then overwhelmed and the structure of the developing bands is prematurely disrupted.

Results have been presented here for only two beds (though a second, more expanded, water-fluidized bed has also been investigated (Anderson 1995)) so we are reluctant to draw general conclusions. However, the numerical solutions are in accord with a number of earlier approximate theoretical results and, in addition to providing some insight into the relation between instability and bubble growth, they do suggest some interesting questions to address in future work. The experimental distinction between bubbling and non-bubbling behaviour does not appear to be an absolute one, and computations should clearly be performed for some systems where the ratio of the solids and fluid densities is intermediate between the two cases studied here. There are long-standing reports of observations of behaviour lying between the two extremes in liquid-fluidized beds of large, very dense particles (Davidson & Harrison 1963) and these could be compared with corresponding solutions of the equations of motion. It is also well known that the tendency to bubble in gas-fluidized beds is reduced significantly as the pressure of the fluidizing gas is increased, and computations could be used to explore whether additional physics needs to be introduced into the equations of motion to explain this. The existence of apparently different mechanisms determining whether bubbles will grow from small perturbations, and whether existing incipient bubbles will survive, raises the question of whether there are systems in which injected bubbles can survive indefinitely, but bubbles will not grow from a uniform fluidized bed. Finally, the present computations have been limited to two-dimensional spatially periodic motions. Similar calculations should be performed for isolated disturbances, both two-dimensional and axially symmetric in three dimensions, to resolve questions about the mutual influence of neighbouring bubbles.

This work has been supported by the National Science Foundation, Fluid, Particulate and Hydraulic Systems Program, under grant number CTS 92-07469. The two-dimensional computations were all carried out on a Cray C-90 supercomputer. This work could not have been accomplished without a generous grant of time from the Pittsburgh Supercomputing Center. K. A. wishes to acknowledge personal support in the form of a National Science Foundation Fellowship. R. J. thanks Trinity College, Cambridge, for an appointment as Visiting Fellow Commoner, and the Department of

Applied Mathematics and Theoretical Physics, Cambridge University for use of its facilities during the later stages of the work. Finally, all of us wish to acknowledge many fruitful discussion, throughout the course of the work, with our colleagues B. Glasser and I. G. Kevrekidis.

REFERENCES

ANDERSON, K. 1995 Instabilities and the formation of bubbles in fluidized beds. PhD dissertation, Princeton University.

ANDERSON, T. B. & JACKSON, R. 1967 Fluid mechanical description of fluidized beds. Equations of motion. *Ind. Engng Chem. Fundam.* **6**, 527–539.

ANDERSON, T. B. & JACKSON, R. 1968 Fluid mechanical description of fluidized beds. Stability of the state of uniform fluidization. *Ind. Engng Chem. Fundam.* **7**, 12–21.

ANDERSON, T. B. & JACKSON, R. 1969 Fluid mechanical description of fluidized beds. Comparison of theory and experiment. *Ind. Engng Chem. Fundam* **8**, 137–144.

BATCHELOR, G. K. 1988 A new theory of the instability of a uniform fluidized bed. *J. Fluid Mech.* **193**, 75–110.

BATCHELOR, G. K. 1993 Secondary instability of a gas-fluidized bed. *J. Fluid Mech.* **257**, 359–371.

BATCHELOR, G. K. & NITSCHE, J. M. 1991 Instability of stationary unbounded stratified fluid. *J. Fluid Mech.* **227**, 357–391.

BATCHELOR, G. K. & NITSCHE, J. M. 1994 Expulsion of particles from a buoyant blob in a fluidized bed. *J. Fluid Mech.* **278**, 63–81.

DANKWORTH, D. & SUNDARESAN, S. 1991 Time-dependent flow patterns arising from the instability of uniform fluidization. Presentation at *Symposium on the Mechanics of Fluidized Beds, 1–14 July 1991*, Stanford University (see also *J. Fluid Mech.* **236**, 477–495).

DAVIDSON, J. F. 1961 Discussion at Symposium on Fluidization. *Trans. Inst. Chem. Engrs* **39**, 230–232.

DAVIDSON, J. F. & HARRISON, D. 1963 *Fluidized Particles*. Cambridge University Press.

DIDWANIA, A. K. & HOMSY, G. M. 1981 Flow regimes and flow transitions in liquid fluidized beds. *Intl J. Multiphase Flow* **7**, 563–580.

DIDWANIA, A. K. & HOMSY, G. M. 1982 Resonant side-band instabilities in wave propagation in fluidized beds. *J. Fluid Mech.* **122**, 433–438.

DREW, D. A. 1971 Averaged field equations for two-phase media. *Stud. Appl. Maths* **50**, 133–166.

DREW, D. A. & SEGEL, L. A. 1971 Averaged equations for two-phase flows. *Stud. Appl. Maths* **50**, 205–231.

EL-KAISSY, M. M. & HOMSY, G. M. 1976 Instability waves and the origin of bubbles in fluidized beds. *Intl J. Multiphase Flow* **2**, 379–395.

FANUCCI, J. B., NESS, N. & YEN, R.-H. 1979 On the formation of bubbles in gas-particulate fluidized beds. *J. Fluid Mech.* **94**, 353–367.

FOSCOLO, P. U. & GIBILARO, L. G. 1984 A fully predictive criterion for the transition between particulate and aggregative fluidization. *Chem. Engng Sci.* **39**, 1667–1675.

GANSER, G. H. & DREW, D. A. 1990 Nonlinear stability analysis of a uniform fluidized bed. *Intl J. Multiphase Flow* **16**, 447–460.

GARG, S. K. & PRITCHETT, J. W. 1975 Dynamics of gas fluidized beds. *J. Appl. Phys.* **46**, 4493–4500.

GIDASPOW, D., SYAMLAL, M. & SEO, Y. C. 1986 Hydrodynamics of fluidization: supercomputer generated vs. experimental bubbles. *J. Powder Bulk Solids Technol.* **10**, 19–23.

GÖZ, M. 1992 On the origin of wave patterns in fluidized beds. *J. Fluid Mech.* **240**, 379–404.

HAFF, P. K. 1983 Grain flow as a fluid mechanical phenomenon. *J. Fluid Mech.* **134**, 401–430.

HARRIS, S. E. & CRIGHTON, D. G. 1994 Solitons, solitary waves, and voidage disturbances in gas-fluidized beds. *J. Fluid Mech.* **266**, 243–276.

HERNANDEZ, J. A. & JIMENEZ, J. 1991 Bubble formation in dense fluidized beds. In *Proc. NATO Advanced Research Workshop on the Global Geometry of Turbulence* (ed. J. Jimenez) pp. 133–142. Plenum.

HINCH, E. J. 1977 An averaged-equation approach to particle interactions in a fluid suspension. *J. Fluid Mech.* **83**, 695–720.

JACKSON, R. 1963*a* The mechanics of fluidized beds. I: the stability of the state of uniform fluidization. *Trans. Inst. Chem. Engrs* **41**, 13–21.

JACKSON, R. 1963*b* The mechanics of fluidized beds. II: the motion of fully developed bubbles. *Trans. Inst. Chem. Engrs* **41**, 22–28.

JOSEPH, D. D. & LUNDGREN, T. S. 1990 Ensemble average and mixture theory equations for incompressible fluid-particle suspensions. *Intl J. Multiphase Flow* **16**, 35–42.

KUIPERS, J. A. M. 1990 A two-fluid micro balance model of fluidized beds. PhD thesis, Twente University of Technology.

LIU, J. T. C. 1982 Note on a wave-hierarchy interpretation of fluidized bed instabilities. *Proc. R. Soc. Lond.* A **380**, 229–239.

LIU, J. T. C. 1983 Nonlinear unstable wave disturbances in fluidized beds. *Proc. R. Soc. Lond.* A **389**, 331–347.

LOCKETT, M. J. & HARRISON, D. 1967 The distribution of voidage fraction near bubbles rising in gas fluidized beds. In *Proc. Intl Symp. on Fluidization* (ed. A. A. H. Drinkenburg), pp. 257–267. Netherlands University Press.

MURRAY, J. D. 1965 On the mathematics of fluidization. Part 1. Fundamental equations and wave propagation. *J. Fluid Mech.* **21**, 465–493.

MUTSERS, S. M. P. & RIETEMA, K. 1977 The effect of interparticle forces on the expansion of a homogeneous gas-fluidized bed. *Powder Technol.* **18**, 239–248.

NEEDHAM, D. J. & MERKIN, J. H. 1983 The propagation of a voidage disturbance in a uniform fluidized bed. *J. Fluid Mech.* **131**, 427–454.

NEEDHAM, D. J. & MERKIN, J. H. 1984 The evolution of a two-dimensional small-amplitude voidage disturbance in a uniformly fluidized bed. *J. Engng Maths* **18**, 119–132.

NEEDHAM, D. J. & MERKIN, J. H. 1986 The existence and stability of quasi-steady periodic voidage waves in a fluidized bed. *Z. Angew. Math. Phys.* **37**, 322–339.

NGUYEN, X. T., LEUNG, L. S. & WEILAND, R. H. 1973 On void fractions around a bubble in a two-dimensional fluidized bed. In *Proc. Intl Congress on Fluidization and its Applications* (ed. H. Angelino, J. P. Couder & H. Gilbert), pp. 230–239. Societe de Chemie Industrielle.

NIGMATULIN, R. I. 1979 Spatial averaging in the mechanics of heterogeneous and dispersed systems. *Intl J. Multiphase Flow* **5**, 353–385.

PIGFORD, R. L. & BARON, T. 1965 Hydrodynamic stability of a fluidized bed. *Ind. Engng Chem. Fundam.* **4**, 81–87.

PRITCHETT, J. W., BLAKE, T. R. & GARG, S. K. 1978 A numerical model of gas fluidized beds. *AIChE Symp. Ser.* 176, vol. 74, pp. 134–148.

RICHARDSON, J. F. & ZAKI, W. N. 1954 Sedimentation and fluidization: Part I. *Trans. Inst. Chem. Engrs* **32**, 35–53.

SYAMLAL, M. & O'BRIEN, T. J. 1989 Computer simulation of bubbles in a fluidized bed. *AIChE Symp. Ser.* 270, vol. 85, pp. 22–31.

TSINONTIDES, S. & JACKSON, R. 1993 The mechanics of gas fluidized beds with an interval of stable fluidization. *J. Fluid Mech.* **255**, 237–274.

WILHELM, R. H. & KWAUK, M. 1948 Fluidization of solid particles. *Chem. Engng Prog.* **44**, 201–218.

YATES, J. G., CHEESMAN, D. J. & SERGEEV, Y. A. 1994 Experimental observations of voidage distribution around bubbles in a fluidized bed. *Chem. Engng Sci.* **49**, 1885–1895.

ZHANG, D. Z. & PROSPERETTI, A. 1994 Averaged equations for inviscid disperse two-phase flow. *J. Fluid Mech.* **267**, 185–219.